11-16-2020

Star Formation in Dwarf Galaxies

Simeon L. Bolds
Florida International University, sbolds@fiu.edu

FLORIDA INTERNATIONAL UNIVERSITY

Miami, Florida

STAR FORMATION IN DWARF GALAXIES

A thesis submitted in partial fulfillment of

the requirements for the degree of

MASTER OF SCIENCE

in

PHYSICS

by

Simeon Bolds

2020

To: Dean Michael R. Heithaus
College of Arts, Sciences and Education

This thesis, written by Simeon Bolds, and entitled Star Formation in Dwarf Galaxies, having been approved in respect to style and intellectual content, is referred to you for judgment.

We have read this thesis and recommend that it be approved.

_____
Peter Markowitz

_____
James Webb

_____
Caroline Simpson, Major Professor

Date of Defense: November 16, 2020

The thesis of Simeon Bolds is approved.

_____
Dean Michael R. Heithaus
College of Arts, Sciences and Education

_____
Andrés G. Gil
Vice President for Research and Economic Development
and Dean of the University Graduate School

Florida International University, 2020

ACKNOWLEDGMENTS

I wish to thank the members of my committee for being patient and supportive during these trying times. It is with their help that I am able to present this thesis in such a fashion. I would also like to give a special thanks to Dr. Caroline Simpson. As my advisor, Dr. Simpson has provided me with a tremendous amount of care and support through a great deal of personal issues during my time at this university. From the beginning, she had confidence in my ability to complete my degree with high standards. It is because of her and her willingness to work with me that a feeling of doubt and loneliness was not a permanent feeling. Both stern and compassionate, Dr. Simpson provided me with the moral support to keep a high level of standard in my work. For these reasons, Dr. Simpson has my gratitude.

ABSTRACT OF THE THESIS

STAR FORMATION IN DWARF GALAXIES

by

Simeon Bolds

Florida International University, 2020

Miami, Florida

Professor Caroline Simpson, Major Professor

A catalog of neutral hydrogen (HI) of nearby dwarf galaxies obtained from the LITTLE THINGS (Local Irregulars That Trace Luminosity Extremes, The HI Nearby Galaxy Survey) project along with ancillary data are used to examine the relative importance of star-induced star formation associated with the HI holes in 31 dwarf galaxies. HI shells/rings surrounding the HI holes are defined and the fractional amounts of HI and star formation in the rings relative to the global galactic amounts are calculated. These are then compared to look for correlations between the amount of star formation and neutral hydrogen in the rings. Two galaxies in the sample have high HI and high Hα fractions consistent with star-induced star formation being an important mechanism in these galaxies. We find that most galaxies fall into low-HI and low-Hα fractions and so star-induced star formation is not important currently.

TABLE OF CONTENTS

LIST OF TABLES

TABLE PAGE

LIST OF FIGURES

FIGURE PAGE

I. INTRODUCTION:

In the 17th Century, the first galaxies were identified by French astronomer Charles Messier, and at that time galaxies only looked like fuzzy objects in the night sky. Nowadays, these fuzzy objects in the sky are being studied in great detail and in more parts of the electromagnetic spectrum than just the visible. Because of ongoing studies, we now know more about how they age and what they create. And though we continue to learn more about galaxies, dwarf galaxies have been studied for less than 100 years.

Since their discovery in 1937 by American Astronomer Harlow Shapley, we know now that dwarf galaxies are the most abundant type of galaxy in the universe [1]. Despite being more abundant they are also more difficult to detect. Dwarf galaxies are low mass objects, ranging from 10^7 to 10^9 solar masses. Their diameters usually range from 0.1-10 kiloparsecs (kpc) and their luminosities range from 10^5 to 10^7 solar luminosities. Dwarf galaxies are generally classified as four main types: dwarf elliptical, dwarf spheroidal, dwarf spiral, and dwarf irregular. Dwarf irregular (dIrr) is a particularly interesting type to look at because they contain a substantial amount of gas and dust and clear evidence of star formation. In addition to those types of dwarf galaxies, we have Blue Compact Dwarfs (BCDs) which are dwarf galaxies that are undergoing higher rates of star formation; leading to more hot, massive, young stars which give them a bluer color and more compact appearance than other dwarf galaxies [2, 3].

Due to the nature of dwarf galaxies, research is hard to do and so there are still unknown qualities of dwarf galaxies. The LITTLE THINGS[1] (Local Irregulars That Trace Luminosity Extremes) project studies dwarf irregular galaxies in order to understand more about star formation within dwarf galaxies [1]. Specifically, the project looks closely at the cause of triggered star formation and its regulation; things that are not too well established in current theories of star formation.

1. NEUTRAL HYDROGEN:

Hydrogen accounts for approximately 74% of matter in the known universe. Because of its abundance in the universe hydrogen is an important tool in determining several qualities in the universe, such as: the study of the chemical make-up and morphology of galaxies and for the purposes of this study, star formation.

Hydrogen commonly consists of one proton and one electron and is called "protium," there are other isotopes which consisted of more particles, but protium is the most common (with an abundance over 99.98%). When protium is neutral, the atom has an equal number of protons and electrons, it is commonly referred to as

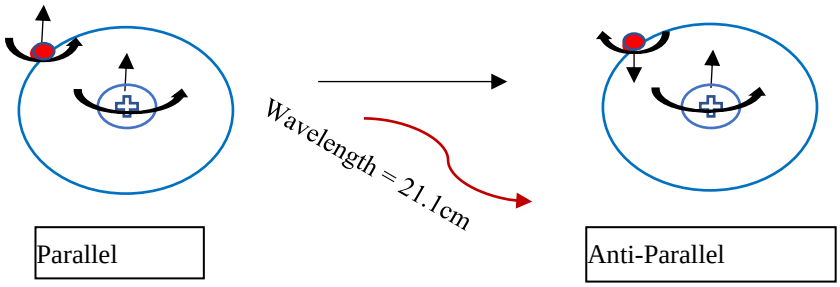

Figure 1: Shows a hydrogen atom - comprised of one proton (white circle with plus sign and one electron (red circle) - with a slightly excited electron on the left whose spin is aligned with the proton eventually flipping its spin to enter a lower energy state. The energy emitted is equal to a wavelength of 21cm.

[1] Local Irregulars That Trace Luminosity Extremes, The H I Nearby Galaxy Survey https://science.nrao.edu/science/surveys/littlethings

"HI." A rare occurrence of HI is a hyperfine transition, commonly referred to as a "spin-flip transition," the electron spin goes from parallel to anti-parallel with the nuclear spin. As the transition happens electromagnetic radiation is released at a wavelength of 21.1cm, as shown in Figure 1, (this is commonly referred to as the "21 cm radiation line"); this wavelength is detectable with radio astronomy. Even though this occurrence is rare, through the abundance of HI astronomers are able to witness this transition and because of this make the necessary measurements and inferences into a galaxy's morphology and star formation.

2. IONIZED HYDROGEN:

HI is relatively easy to ionize (to become HII), and after ionization the electron will recombine with a different proton, and as this energetic electron is captured, this newly excited hydrogen not being able to exist in such a state for too long must come down to its ground state. In this transition, the electron cascades down from its excited state (n >1) to its ground state (n=1). A certain electron transition, n=3 to n=2, emits "Hα photons" (releases a photon of wavelength 656.284 nm, which is a deep red color) [4]. And though the newly excited hydrogen's electron can exist in any excited state before cascading down, the majority of the time its transitions will include n=3 to n=2, which makes Hα emission a good tracer of these HII regions and can be used to give us valuable insight into ongoing star formation.

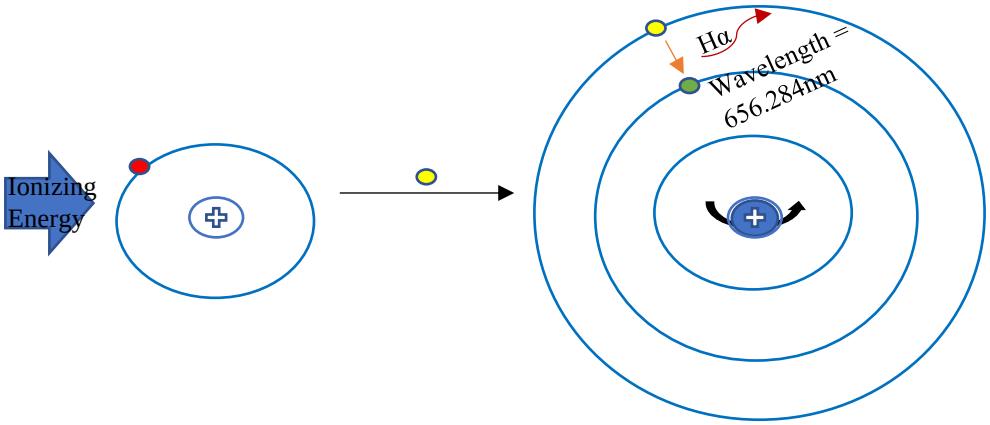

Figure 3: Shows a hydrogen atom being ionized and then the free electron (yellow dot) being captured by a free proton and de-exciting releasing an Hα emission.

3. STAR FORMATION:

A. INTERSTELLAR MEDIUM

The Interstellar Medium, hereby referred to as "ISM," contains about 10-15% of the matter in most star-forming galaxies by mass. The ISM is comprised of:

- cold atomic hydrogen – where HI 21 cm line absorption occurs
- warm atomic hydrogen – where HI 21 cm line emission occurs
- warm ionized hydrogen – where Hα emissions occur (see section I.2)
- Hot ionized gas – where X-ray emission and absorption by ionized metals occur
- molecular clouds – where radio and infrared molecular emissions and absorptions occur

Roughly half of the mass of the ISM is found within the molecular clouds. Additionally, molecular clouds are the site for star formation to occur.

B. MOLECULAR CLOUD

A molecular cloud is a cold interstellar cloud in which the formation of molecules occurs, most commonly molecular hydrogen, as opposed to other areas of the ISM that contain ionized gas. Inside the molecular cloud there are highly dense areas called “clumps.”

The process of star formation starts within molecular clouds when these clumps are perturbed due to some event (i.e.: shocks from supernovae, spiral density waves, or turbulence) that causes the gravitational force to overtake the gas pressure allowing for these clumps to collapse.

As the gas collapses it also begins to heat up; usually these photons are able to escape allowing the cloud to radiate energy. Though some energy is able to be given off, not all the energy is radiated off and the inner workings of a core begin. Eventually the core becomes so dense that the energy radiating from within is unable to get through, it is at this point that the cloud becomes optically opaque (which is why radio astronomy is helpful), and the temperature of the core continues to increase [5].

C. PROTOSTAR

A protostar is one of the earlier stages of a star. This stage of a star’s life begins during the collapse of the gas clump as the opaque core forms. During this

phase, the central core continues to gather mass from the molecular cloud in which it started in. As the core continues to gain mass from the infalling gas, eventually thermonuclear fusion begins to happen.

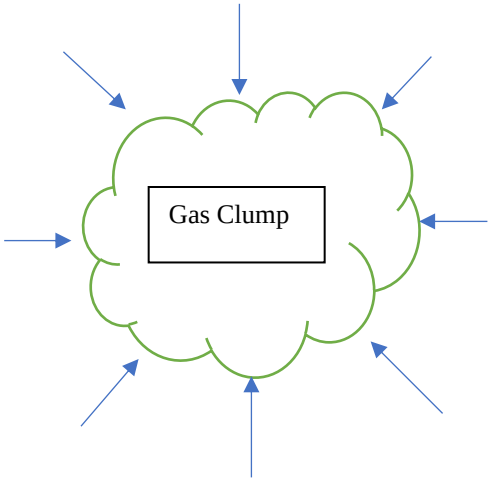

D. BECOMING A MAIN SEQUENCE STAR

After a protostar has accreted enough mass to ignite the hydrogen burning process of a star, strong stellar winds are present and along with the hot stellar surface the surrounding HI is ionized to HII, as shown in Figure 3. This phase is more commonly seen with lower mass stars but has been seen in stars as massive as B-type[2] stars. More massive stars, O-type, have such a short period in the phase that they are not observed and are typically seen to just be at the appropriate position in the main-sequence.

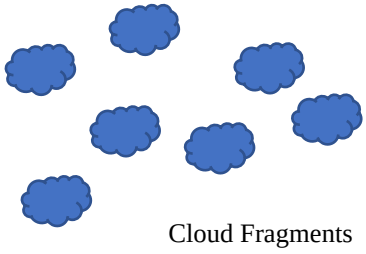

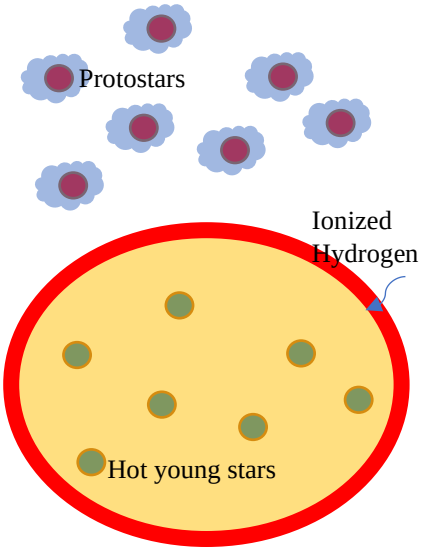

[2] Stellar classification of stars is based on spectral characteristics and listing them from the hottest and most luminous to the least would go as O, B, A, F, G, K, M. From the letter categorizations there are also numerical intervals notation from 0 (hottest) to 9 (coolest). There is also a mass sequence, with O stars being the most massive and M stars being the least.

After core fusion is well-established the stellar wind phase ends, and the star becomes a main-sequence star, fusing H to helium (He) in its core for the majority of its life. High mass stars have shorter lifetimes of a few million years, while low mass stars can spend billions of years in this stage.

E. STAR DEATH AND REBIRTH

After an appropriate amount of time on the main sequence, a star will begin to drift into the later stages of its life as a giant[3]. Less massive stars, like our sun, will eject their outer layers and cool, eventually becoming white dwarfs. More massive stars, at least 8 times the mass of our star (O and B type stars), will go supernova. At the ending stages of a star's life, the core is not able to fuse heavier elements and gravity overtakes the thermal and radiation pressure from the star. The outer layers of the star begin to collapse in on itself heating up, as the core reaches a certain temperature photodisintegration happens. Photodisintegration is when the iron nuclei breaks up into alpha particles. With the temperature of the core continuing to rise electrons and protons combine into neutrons. Once the core reaches nuclear densities, a strong force repulsion and neutron degeneracy pressure stop the star from continued contraction. The outer layers of the star that were once falling inward onto the core are then ejected "pushed outwards" by the neutrinos that were created by the neutron creation in the core. This ejection is what we see as a supernova. Since stars form in clusters, the more massive stars that also have a shorter life cycle tend to also experience

[3] There are various giant categories ranging from giants to hypergiants and the mass of a star dictates which giant it will be, because not all stars become giants and not all stars become hypergiants.

their deaths around the same time. These multiple supernovas or “Super supernovae” as coined by Hinderman [6], can blow out a large area of HI in the interstellar medium (see Figure 4). These blowouts are what are known as: “Holes,” “Supershells,” or “Superbubbles” [7].

Hole creation blow-outs create a shockwave that can start the formation of more stars. This process is called star-induced star formation. During this kind of star formation, the shockwave begins the process of star formation by compressing the cold gas in a nearby molecular cloud, which in turn allows for the cloud to fall in on itself creating a new region for star formation to occur [4, 7]. In addition to star-induced star formation, star formation can occur due to random motions in the molecular cloud. These random motions are known as “turbulence” and like star-induced star formation, turbulence can kick start the star formation process by causing areas of the molecular cloud to experience strong compressions that would in turn spark a new region of star formation [8].

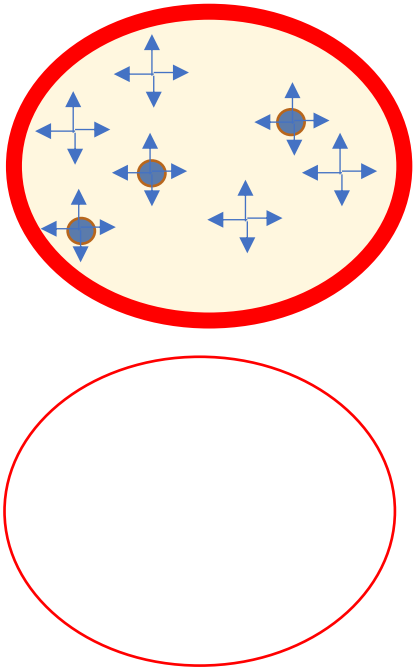

Figure 4: The top image shows a crude direction pattern (blue arrows) of blowout cause by each hot young star (blue). The bottom image shows the encompassed area cleared out of HI from the multiple supernova that occurred.

4. LITTLE THINGS AND THE PROJECT OUTLINE

A. LITTLE THINGS

The LITTLE THINGS project is a multi-wavelength survey that is centered around HI emission line data from the National Radio Astronomy Observatory (NRAO) Very Large Array (VLA)[4]. The HI-line data is characterized by high sensitivity (≤1.1 mJy/beam per channel), high spectral resolution (≤2.6 km/s), and high angular resolution (~6”). Hα images were obtained using the Lowell 1.8m Perkins telescope using a TI CCD and a 32 Angstrom FWHM interference filter and 95 Angstrom off-band filter [1]. The LITTLE THINGS project contains 41 dwarf galaxies. Of the 41, 37 are dIrr and the other 4 are BCDs of various morphologies. These galaxies are nearby (≤10.3Mpc: 6” is 300pc), are known to have atomic hydrogen, and are of a multitude of dwarf galactic properties. Additionally, the LT project includes data from the Galaxy Evolution Explorer (GALEX) in Far-Ultra Violet (FUV) [1], ground based UBV and JHK from the Lowell Observatory facilities [9], and Spitzer satellite mid-infrared (mid-IR). The GALEX UV data traces star formation over the past 100-200 Myr and the UBV data trace star formation over the past 1 Gyr. [10] The JHK and mid-IR data show star formation integrated over a galaxy’s lifetime [9].

[4] NRAO is a facility of National Science Foundation operated under cooperative agreement by Associated Universities, Inc.

B. PREVIOUS STUDY

Using the data obtained by the LITTLE THINGS project, Pokhrel [2] studied holes in the ISM and the HI "porosity" (the 2D and 3D percentages of the galaxies occupied by holes) with their effect on star formation in dwarf galaxies. This study included measuring the kinematics of HI holes/shells in dwarf galaxies and used three different classification of holes based on work by Bagetakos et al. [11]:

- Type 1: Completely blown out holes (no visible gas on either side of the hole in its position-velocity map)
- Type 2: Partially blown out holes (visible gas on only one side of the hole in its position-velocity map)
- Type 3: Intact holes (visible gas on both sides of the hole in its position-velocity map)

By comparing the energy required to produce the HI holes in his galaxy sample to their global star formation rates Pokhrel [2] found that the HI holes were consistent with being formed from episodes of star formation.

C. PROJECT OUTLINE

In this thesis, we further examine star formation in dwarf galaxies using the data collected by the LITTLE THINGS project to study the neutral hydrogen (HI) and excited hydrogen (HII) regions of these dwarf galaxies. We are specifically looking at the HI and Hα emissions to see how much of the current star formation was likely caused by previous star cluster blowouts – how likely

star formation in dwarf galaxies is due to star-induced star formation. We are doing this by:

- Measuring the HI "mass fraction" in the rings (2D shells) around the edges of the HI holes identified in the HI hole catalog [2]. The HI mass fraction is the amount of HI (total integrated flux) in a shell divided by the total amount of HI in the galaxy. The galactic HI mass fraction is then calculated by dividing the sum of the HI in the rings by the total amount of HI in each galaxy.
- Measuring the amount of Hα in the HI rings to calculate the recent star formation rate (SFR). This is used the calculate the SFR fraction in the rings in the same manner as for the HI mass fractions, but using Hα sums.

The presence of HI-rich shells around HI holes as indicated by higher HI mass fractions should be conducive to star formation if an appropriate triggering event such as shocks and energy-input from previous star cluster formation occurs. If we see higher HI mass fractions associated with higher Hα fractions in the rings (Case 1: High-High) this is consistent with the idea of star-induced star formation resulting from the event that created the HI hole. However, if there is little/no star formation in the rings (low Hα fractions) despite higher HI mass fractions (HI-rich rings; Case 2: High-Low), that would indicate that star-induced star formation is not occurring in this case, and is not an important mechanism for star formation in such a galaxy currently.

Low HI mass fractions (HI-poor rings) and high Hα fractions in the rings (Case 3: Low-High) although less conclusive than star formation in the presence of HI-rich rings, could also indicate that that star-induced star formation has taken place in the past 10 Myr; but in this case, the HI would have already been used up or pushed further out by the star formation occurring in the rings. This could be further examined by seeing whether there is a correlation between the hole type and/or age – this would be expected to indicate a more evolved event.

In the case of HI-poor rings with little/no star formation (low HI mass fractions and low Hα fractions: Case 4, Low-Low), we cannot tell whether or not star-induced star formation has been important as a mechanism. If the hole is relatively young, there may not yet have been enough time for HI to be swept into a dense ring or for star formation to have been triggered there. Conversely, if the hole was formed long ago (more than 10 Myr ago), there may have been sufficient time for any triggered star formation in the rings to have stopped. Any massive stars formed (the source of the Hα emission used to detect recent/on-going star formation) would have exploded as supernova already; and as in the case mentioned above, the HI in the rings would have been used up, ionized, or blown out further by the star formation. Similarly, correlations between hole type and/or age could shed light on this. If a hole is young and intact, yet has little HI and little/no star formation in the rings, it would indicate that star-induced star formation has not occurred.

II. DETECTION METHOD

1. THE COMMON ASTRONOMY SOFTWARE APPLICATIONS PACKAGE

The Common Astronomy Software Applications package (CASA[5]) is developed for use with data obtained using radio astronomical telescopes such as the Very Large Array (VLA) and Atacama Large Millimeter Array (ALMA) by members of the National Radio Astronomical Observatory (NRAO), the European Southern Observatory (ESO), the National Astronomical Observatory of Japan (NAOJ), the Academia Sinica Institute of Astronomy and Astrophysics (ASIAA), the CSIRO (Commonwealth Scientific and Industrial Research Organization) division for Astronomy and Space Science (CASS), and the Netherlands Institute for Radio Astronomy (ASTRON). Several tasks can be used to visualize and manipulate data; for the purposes of this study we used "imview" and "ia.rotate".

- Imview- A task that allows for the visualization of FITS[6] formatted files or CASA rendered files. The images can be viewed in various colors to display intensity profiles. In addition to the display of intensity profiles, this task also has the ability to place circles (and other shapes if need be) on an image and then obtain a variety of information from within the area such as intensity sum, average, etc.. This function allows for us to determine ring size and information.

[5] The Common Astronomy Software Applications package; https://casa.nrao.edu/

[6] Flexible Image Transport System

- Ia.rotate – A function that allows for the user to rotate the image allowing for the placement of circles and/or ellipses that are not of 0, 90, or 180 degrees position angle.

2. RING IDENTIFICATION

The ring detection method used the catalog of HI holes created by Nau Raj Pokhrel in his dissertation [2] and described above. Using the cataloged holes, the rings were then determined by using the integrated HI map of the galaxy and measuring the intensity across the semi-major and semi-minor axis of the circle or ellipse to find the lowest points of intensity (indicating the hole and inner portion of the ring) and the cut-off of the higher points of intensity (indicating the edge of the ring) as shown in Figure 5.

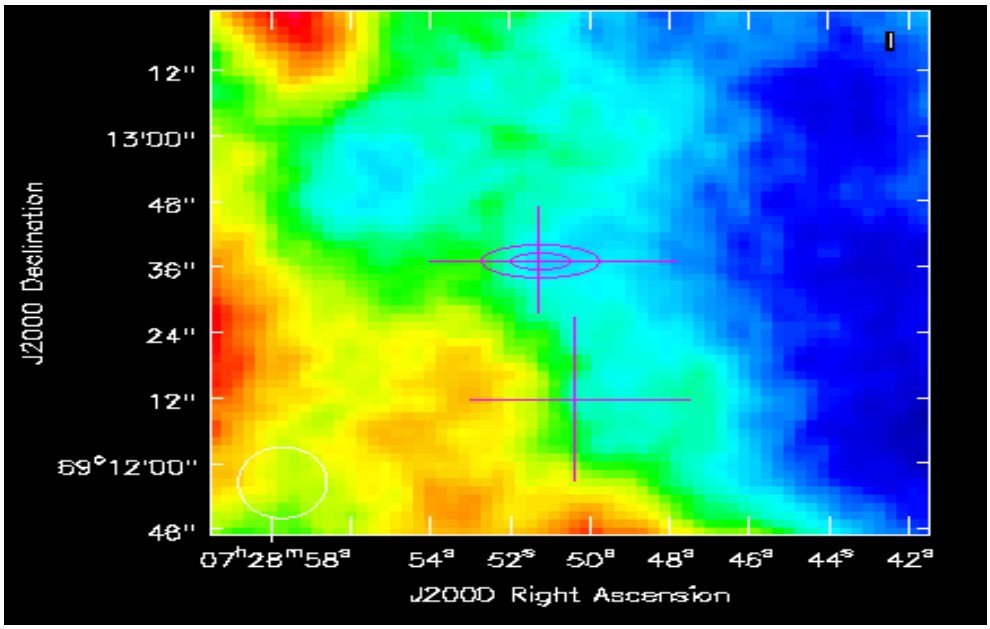

Figure 5: A screenshot from our study in CASA showing the inner and outer definitions of the ring (pink circles) as well as the sem-imajor and sem-iminor splices that would lead to Figure 6.

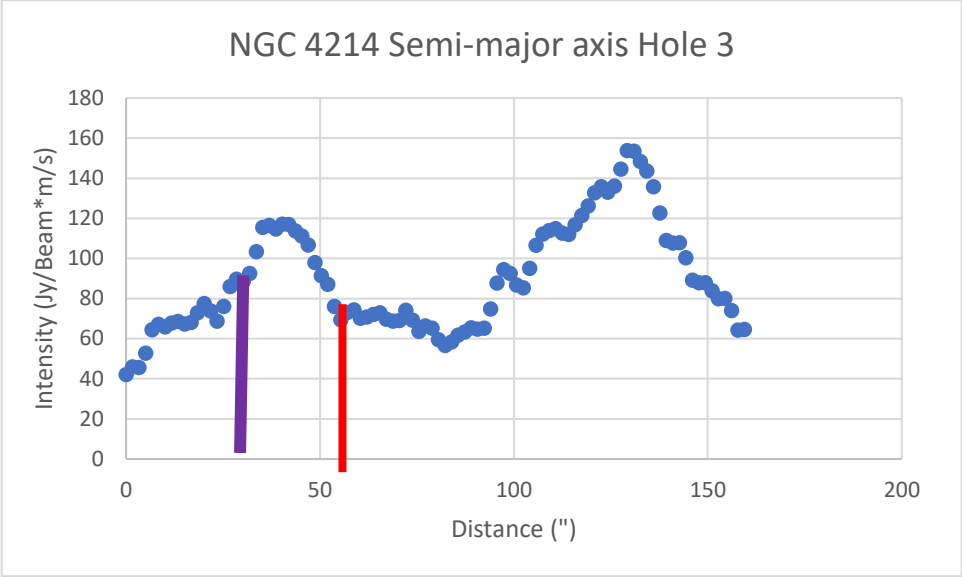

Figure 6: Graph obtained from the sem-imajor axis of hole 3 from NGC 4214. The red line shows the inner region edge and the purple line shows the outer edge of the ring.

3. RING HI AND HA MEASUREMENTS

Using the data from the LITTLE THINGS project, CASA, and the holes cataloged we then:

- Obtained the total amounts of HI and Hα:
    - With the regions defined, the amount of HI and Hα emissions are measured in both regions and the inner region sum is subtracted from the outer region sum to obtain the amount of emission in the ring.
- Obtained the HI mass fraction in rings from HI emissions:
    - The ring's HI emission was converted to HI mass fraction using:

$$M_{HI}(M_{\odot}) = .0245 m_{HI} V$$

Where V is the volume of the hole obtained using a spherical assumption, and m_{HI} is the midplane density obtained from equation using the column density, N_{HI}, and the effective thickness, l:

$$m_{HI} = \frac{N_{HI}}{(3.08 * 10^{18}) * l(r)}$$

With the effective thickness being defined by the galaxy's scale height, Z_0, and inclination, i, as:

$$l(r)(pc) = \frac{Z_0\sqrt{2\pi}}{\cos(i)}$$

And the column density being defined by the brightness temperature, T_B, multiplied by a constant:

$$N_{HI}(cm^{-2}) = 1.82 * 10^{18} T_B$$

All equations used here are from Pokhrel's 2016 dissertation [2].

- Obtained the star formation rates in rings from Hα amounts:
    - The ring's Hα emission was then converted to a star formation rate using the relation in Hunter & Elmegreen [1] where the luminosity from the Hα image is then multiplied by a constant:

$$\dot{M} = 5.96 * 10^{-42} L_{H\alpha} M_{\odot} yr^{-1}$$

These values indicate the amount of star formation occurring in the ring.

- Compared the HI present in the rings and the star formation rates in the ring to the global galactic rates:

- The amount of HI in the rings is compared to the amount of HI in the entire galaxy (the global galactic amount) to estimate how much of the galaxy's HI is contained in the rings. This is also a measure of how HI-rich the rings are.
- The star formation rates in the rings are compared to the rate in the entire galaxy to estimate how much of the global star formation is due to the star formation in the rings.

III. ANALYSIS

1. DATA

Below are the results of our measurements of the HI mass fractions and fractional star formation rates in the rings compared to the global SFR in each galaxy. They are labeled here as "Hα" for brevity. These measurements are broken down by the Hole Type as determined by Pokhrel [2], and the sum total from all the holes is also listed and graphed. As a reminder, Type 1 holes are considered completely blown out, Type 2 are partially blown out (one side intact), and Type 3 are intact holes.

It is worth noting that for our Hα calculations we assume a maximum error of 25% that comes from the calibration uncertainty estimate from Hunter & Elmegreen [1]. Our estimated error of the HI is assumed to be at a maximum of 10% as calculated by Pokhrel in their catalog of the HI holes [2]. These uncertainties are not included in the tables below, but are the basis of the error bars in Figure 7.

The following galaxies were not included due to the lack of Hα emission being present: DDO210, M81dwA, LGS3, F564-V3. DDO 63 and NGC 3738 were also excluded due to these galaxies being face-on (i = 0), this characteristic makes it unable for us to calculate the HI mass content of the rings (see Section 3) thus not allowing us to compare the star formation with the mass content. DDO 50 was also excluded from this study. This is an extremely well-studied galaxy, and the large number of HI holes (41) make it more appropriate for a separate project. This is mentioned in the Future Work section below.

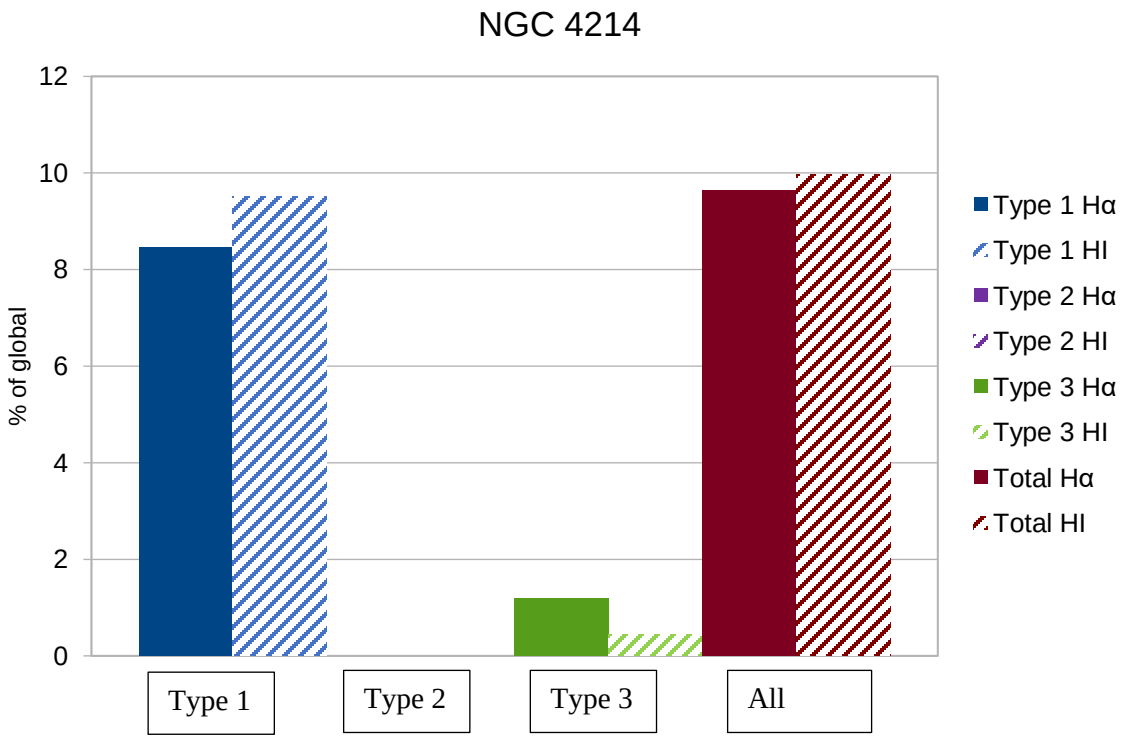

Figure 7: NGC 4214 global percentage of Ha (solid) and HI (striped) contained in the rings.

Table 1: NGC 4214 ring characteristics.

NGC 4214	# of holes	% of global on average per hole type	% of global in total per hole type
Type 1 Hα	9	0.939	8.45
Type 2 Hα	0	…	…
Type 3 Hα	2	0.596	1.19
All holes Hα	11		9.64
Type 1 HI	9	0.793	9.52
Type 2 HI	0	…	…
Type 3 HI	2	0.0994	0.454
All holes HI	11		9.98

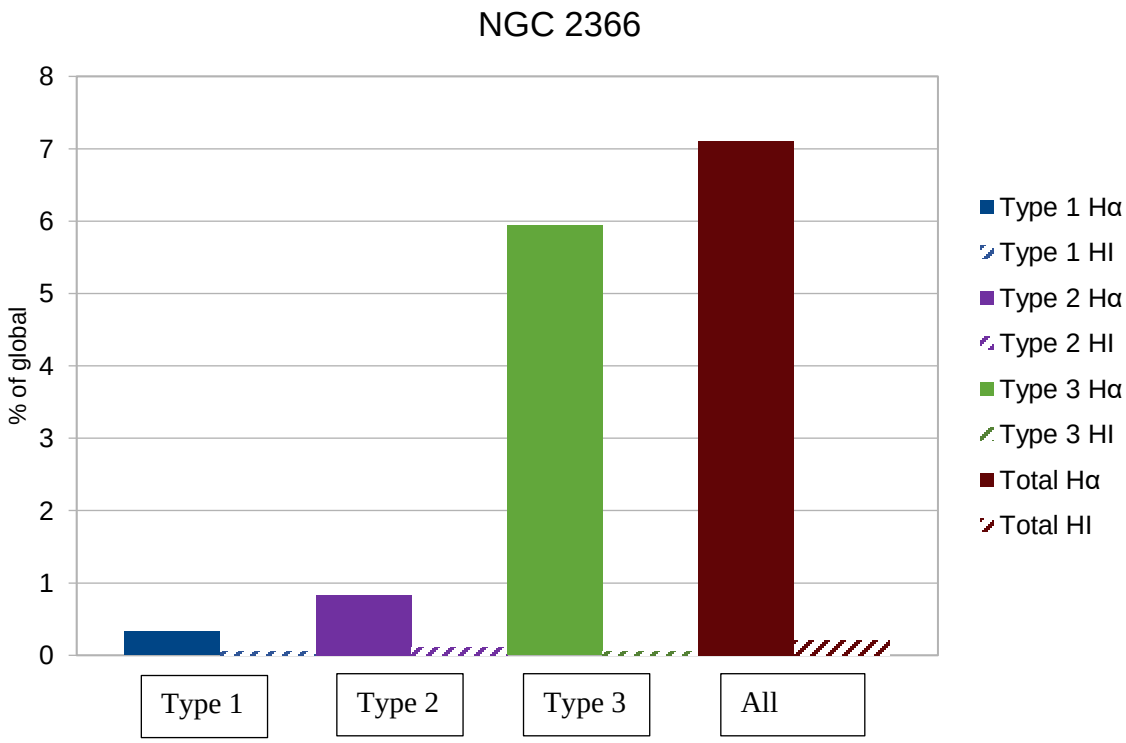

Figure 8: NGC 2366 global percentage of Ha (solid) and HI (striped) contained in the rings.

Table 2: NGC 2366 ring characteristics.

NGC 2366	# of holes	% of global on average per hole type	% of global in total per hole type
Type 1 Hα	4	0.0828	0.331
Type 2 Hα	4	0.208	0.831
Type 3 Hα	2	2.97	5.94
All Holes Hα	10		7.10
Type 1 HI	4	0.00338	0.0528
Type 2 HI	4	0.0103	0.105
Type 3 HI	2	0.0121	0.0544
All Holes HI	10		0.212

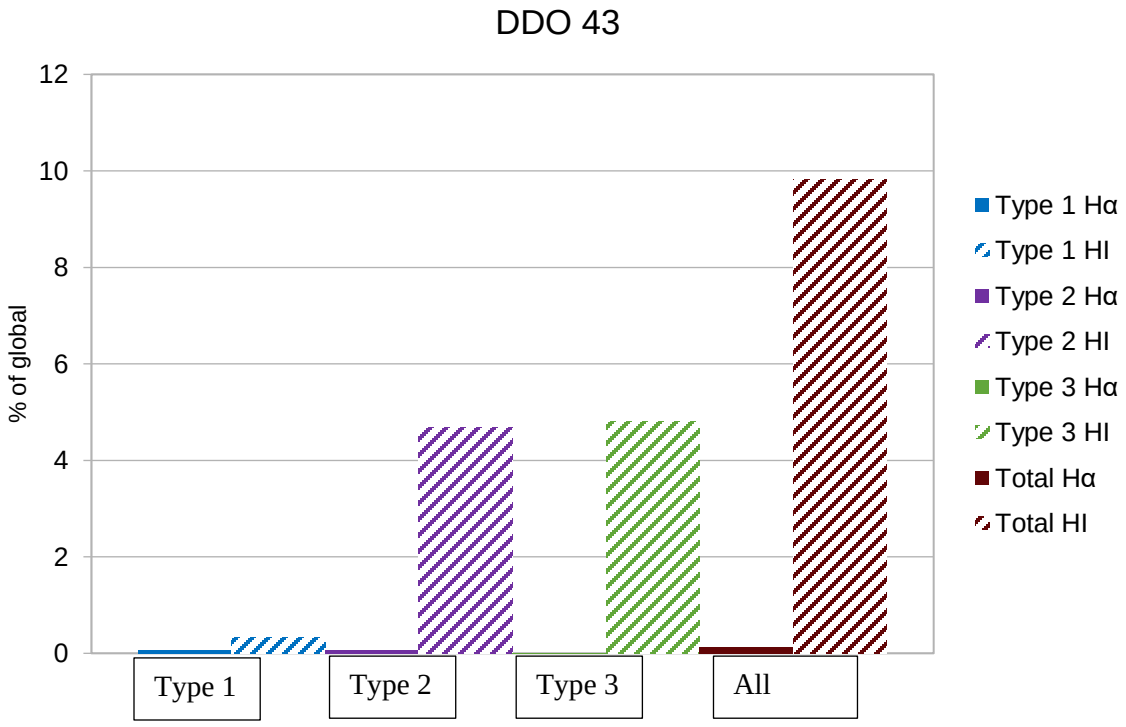

Figure 9: DDO 43 global percentage of Ha (solid) and HI (striped) contained in the rings.

Table 3: DDO 43 ring characteristics.

DDO 43	# of holes	% of global on average per hole type	% of global in total per hole type
Type 1 Hα	1	0.0686	0.0687
Type 2 Hα	8	0.00770	0.0616
Type 3 Hα	6	0.0349	0.00582
All Holes Hα	15		0.136
Type 1 HI	1	0.334	0.334
Type 2 HI	8	0.585	4.68
Type 3 HI	6	0.800	4.80
All Holes HI	15		9.81

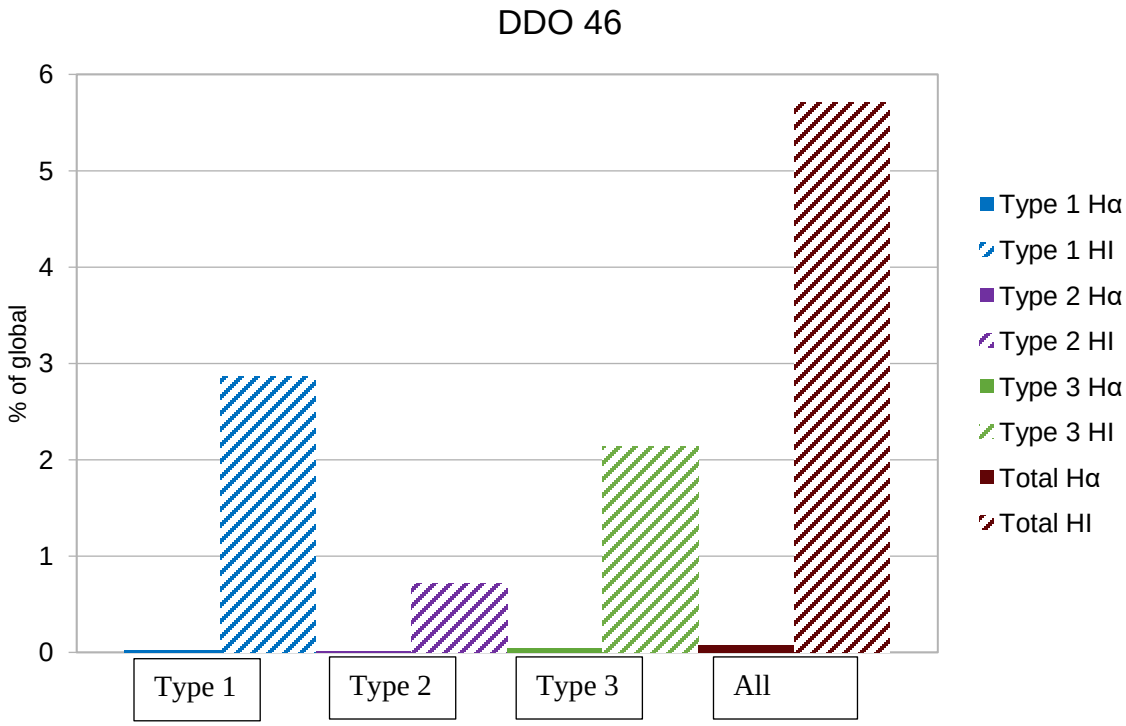

Figure 10: DDO 46 global percentage of Ha (solid) and HI (striped) contained in the rings.

Table 4: DDO 46 ring characteristics.

DDO 46	# of holes	% of global on average per hole type	% of global in total per hole type
Type 1 Hα	3	0.00706	0.0212
Type 2 Hα	5	0.00311	0.0156
Type 3 Hα	10	0.00410	0.0410
All Holes Hα	18		0.0778
Type 1 HI	3	0.953	0.334
Type 2 HI	5	0.180	4.68
Type 3 HI	10	0.213	4.80
All Holes HI	18		5.71

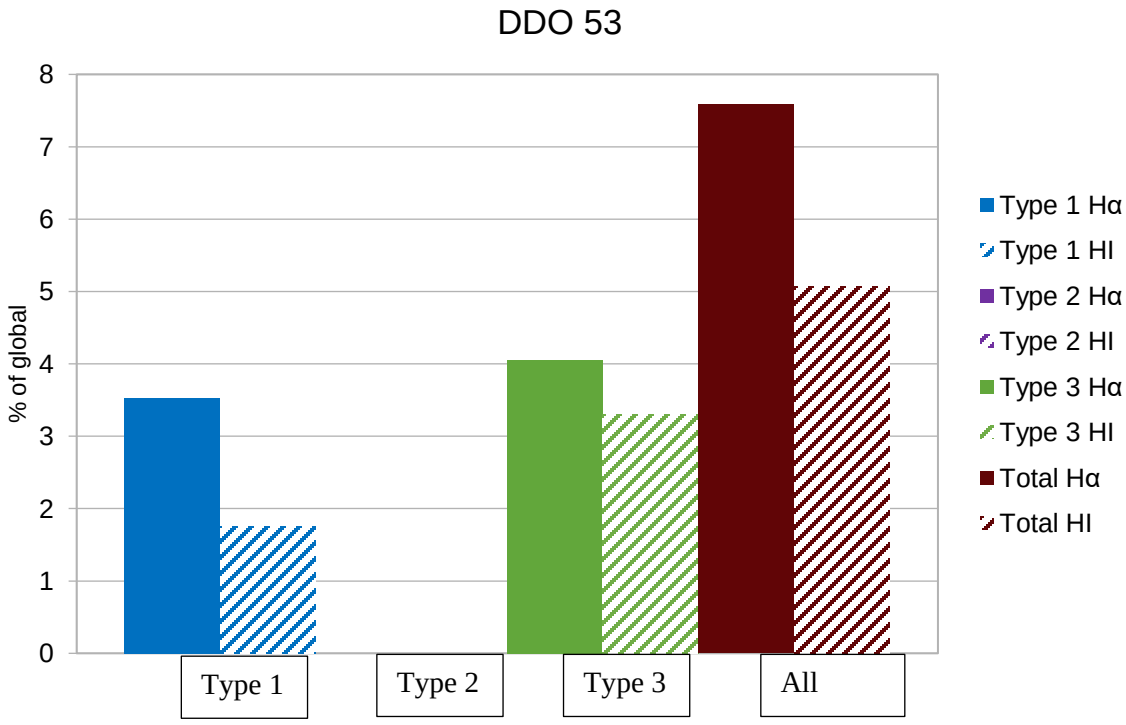

Figure 11: DDO 53 global percentage of Ha (solid) and HI (striped) contained in the rings.

Table 5: DDO 53 ring characteristics.

DDO 53	# of holes	% of global on average per hole type	% of global in total per hole type
Type 1 Hα	1	3.53	3.53
Type 2 Hα	0	…	…
Type 3 Hα	6	0.676	4.06
All Holes Hα	7		7.58
Type 1 HI	1	1.76	1.76
Type 2 HI	0	…	…
Type 3 HI	6	0.662	3.31
All Holes HI	7		5.07

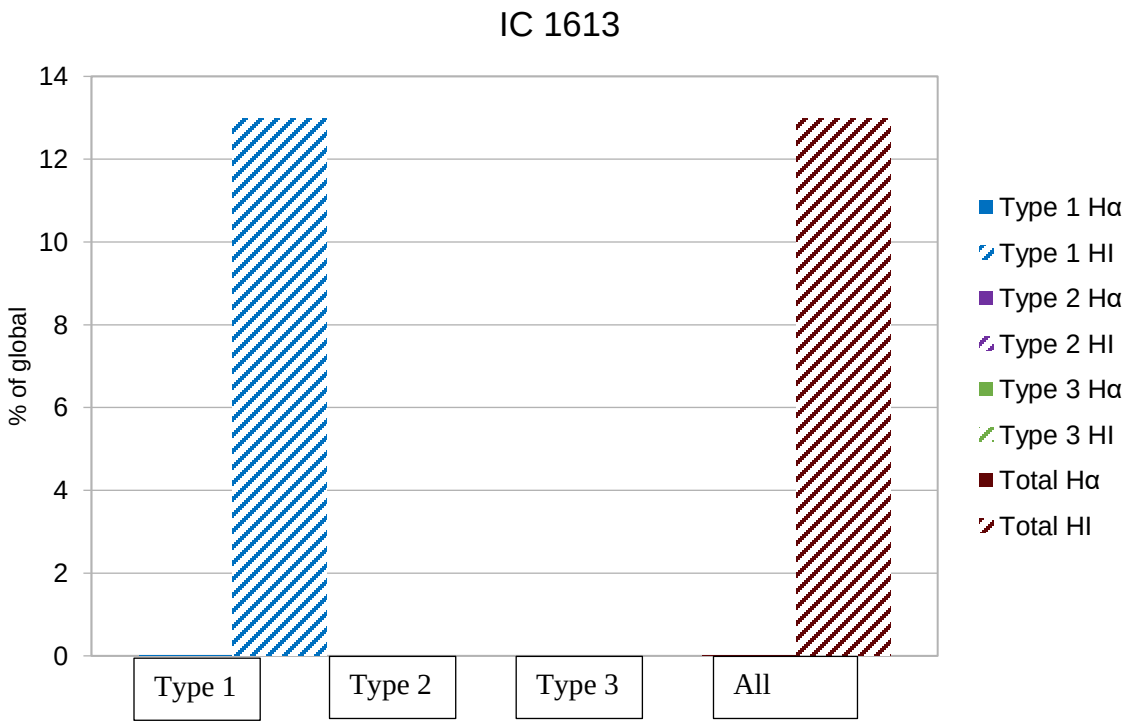

Figure 12: IC 1613 global percentage of Ha (solid) and HI (striped) contained in the rings.

Table 6: IC 1613 ring characteristics.

IC 1613	# of holes	% of global on average per hole type	% of global in total per hole type
Type 1 Hα	11	0.00146	0.0161
Type 2 Hα	…	…	…
Type 3 Hα	…	…	…
All Holes Hα	11		0.0161
Type 1 HI	11	1.85	12.9
Type 2 HI	…	…	…
Type 3 HI	…	…	…
All Holes HI	11		12.9

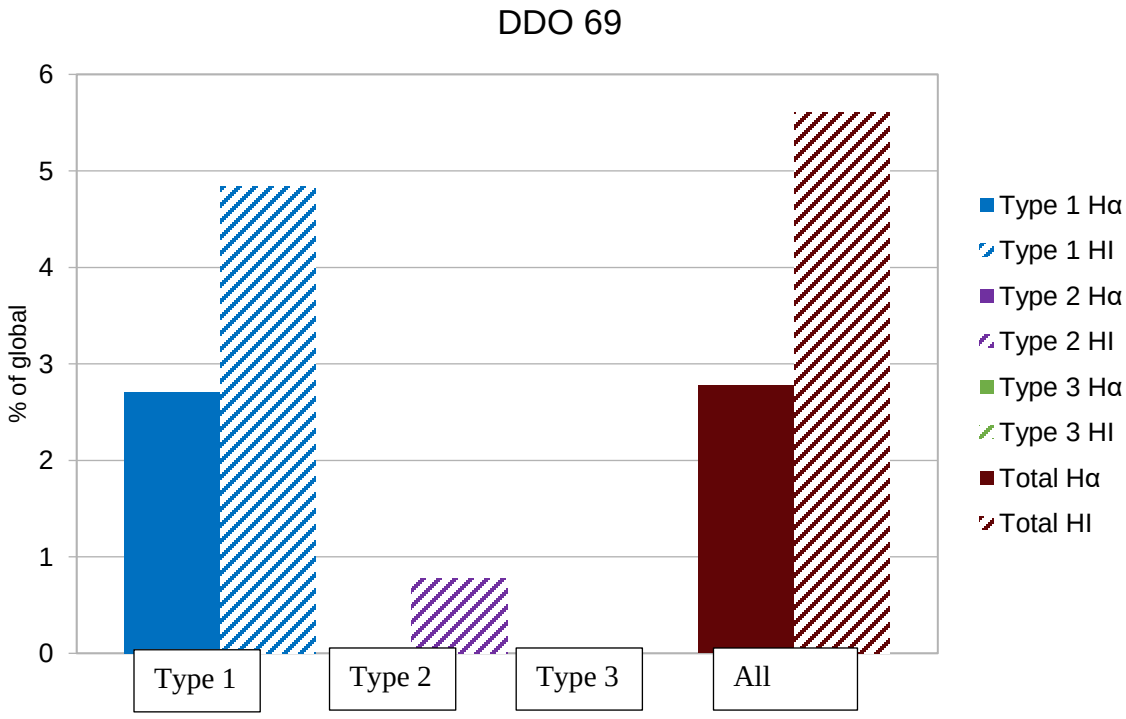

Figure 13: DDO 69 global percentage of Ha (solid) and HI (striped) contained in the rings.

Table 7: DDO 69 ring characteristics.

DDO 69	# of holes	% of global on average per hole type	% of global in total per hole type
Type 1 Hα	2	1.35	2.71
Type 2 Hα	2	0.00	0.00
Type 3 Hα	…	…	…
All Holes Hα	4		2.77
Type 1 HI	2	2.42	4.83
Type 2 HI	2	0.388	0.776
Type 3 HI	…	…	…
All Holes HI	4		5.61

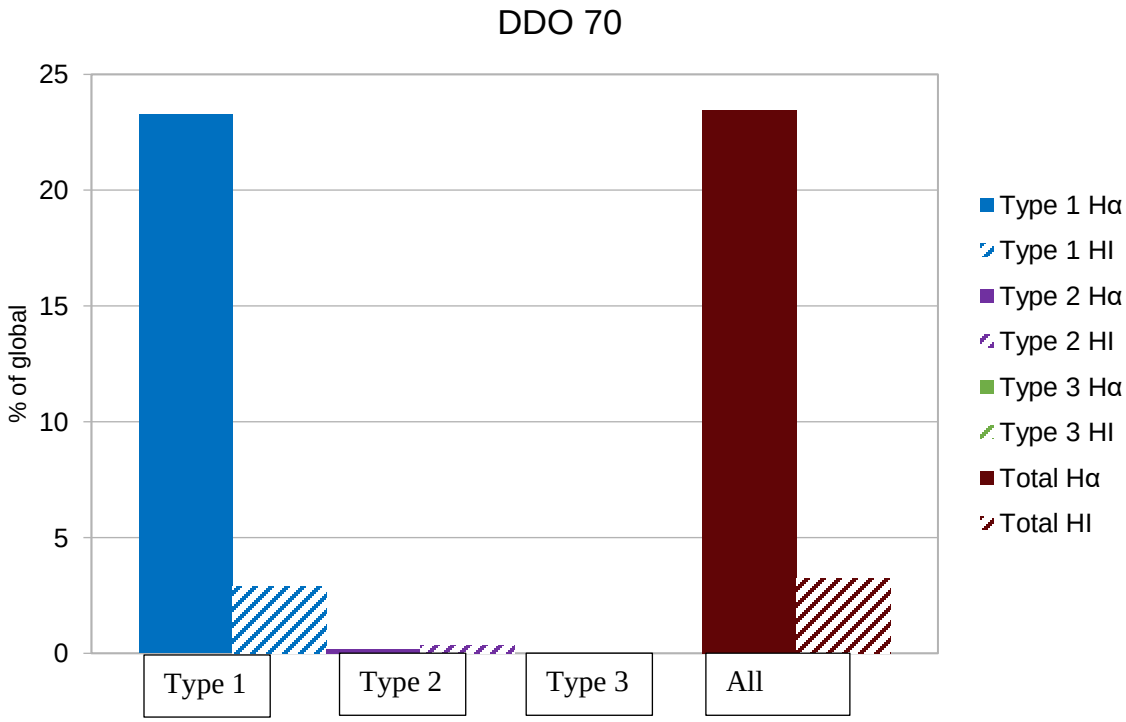

Figure 14: DDO 70 global percentage of Ha (solid) and HI (striped) contained in the rings

Table 8: DDO 70 ring characteristics.

DDO 70	# of holes	% of global on average per hole type	% of global in total per hole type
Type 1 Hα	8	2.91	23.3
Type 2 Hα	1	0.189	0.189
Type 3 Hα	…	…	…
All Holes Hα	9		23.3
Type 1 HI	8	0.481	2.88
Type 2 HI	1	0.349	0.349
Type 3 HI	…	…	…
All Holes HI	9		3.2

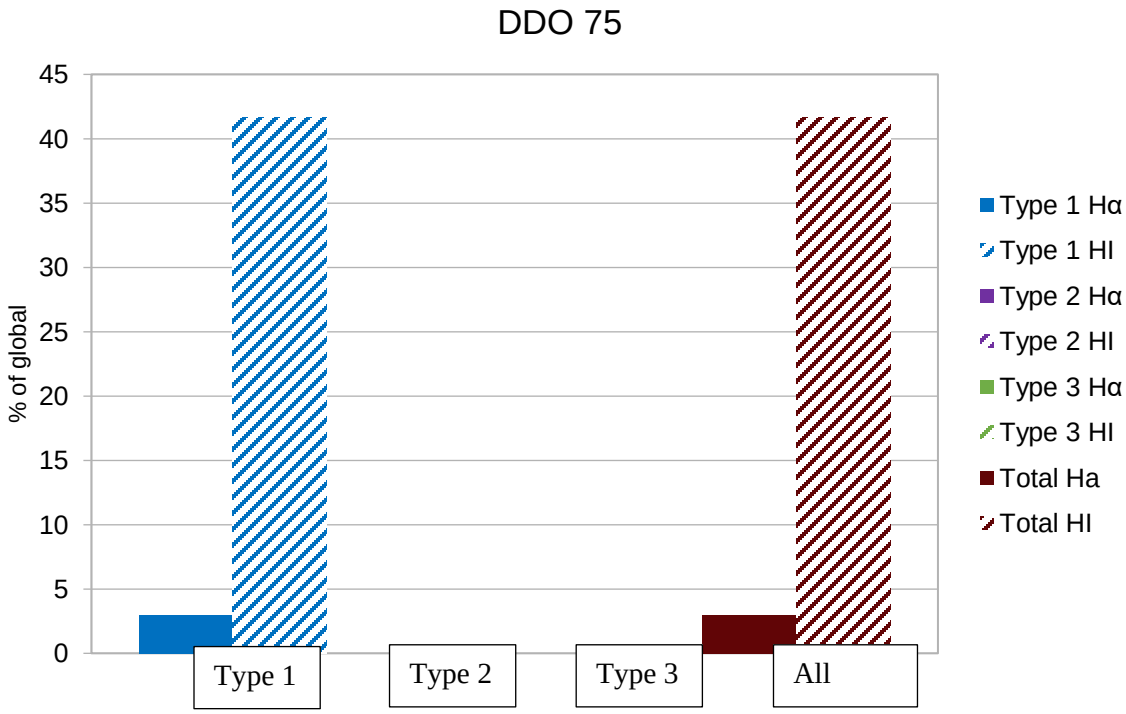

Figure 15: DDO 75 global percentage of Ha (solid) and HI (striped) contained in the rings

Table 9: DDO 75 ring characteristics.

DDO 75	# of holes	% of global on average per hole type	% of global in total per hole type
Type 1 Hα	4	0.744	2.98
Type 2 Hα	…	…	…
Type 3 Hα	…	…	…
All Holes Hα	4		2.98
Type 1 HI	4	10.4	41.7
Type 2 HI	…	…	…
Type 3 HI	…	…	…
All Holes HI	4		41.7

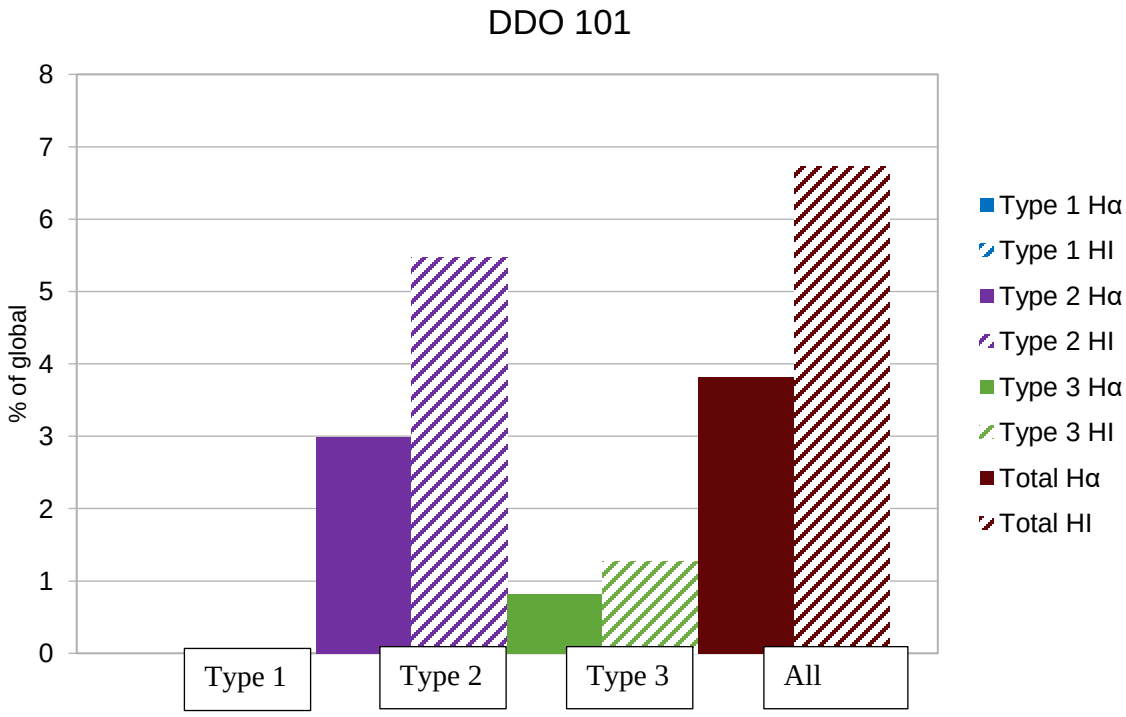

Figure 16: DDO 101 global percentage of Ha (solid) and HI (striped) contained in the rings.

Table 10: DDO 101 ring characteristics.

DDO 101	# of holes	% of global on average per hole type	% of global in total per hole type
Type 1 Hα	…	…	…
Type 2 Hα	1	2.99	2.99
Type 3 Hα	1	0.820	0.820
All Holes Hα	2		3.81
Type 1 HI	…	…	…
Type 2 HI	1	5.47	5.47
Type 3 HI	1	1.27	1.27
All Holes HI	2		6.73

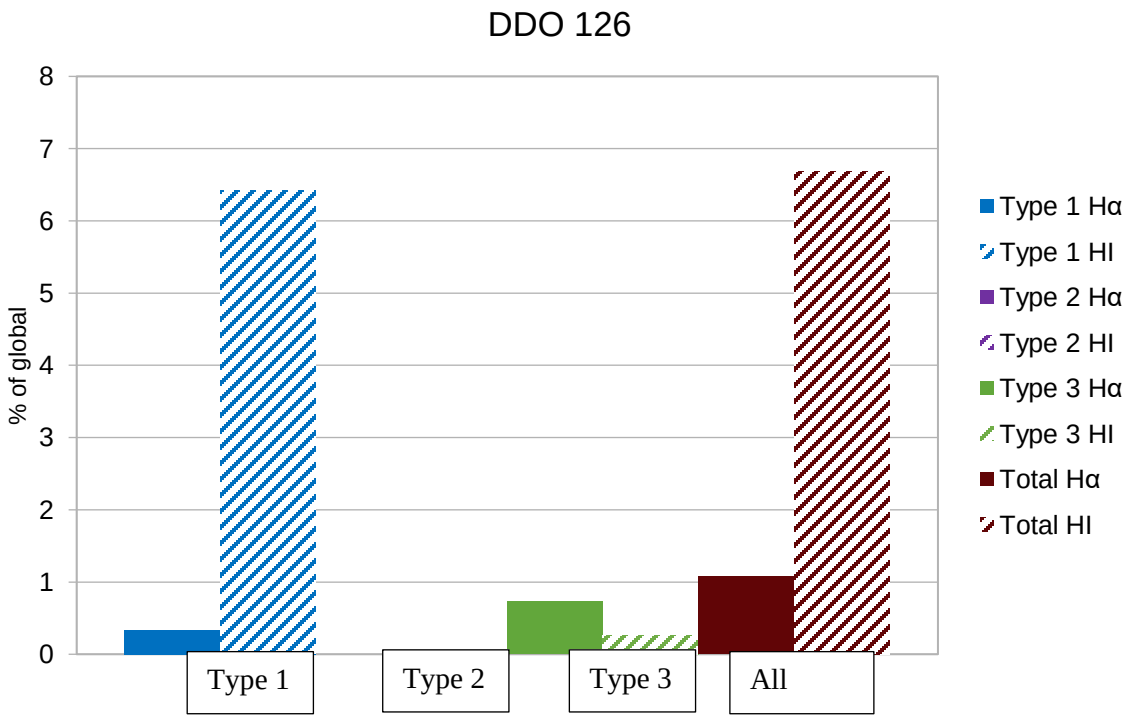

Figure 17: DDO 126 global percentage of Ha (solid) and HI (striped) contained in the rings.

Table 11: DDO 126 ring characteristics.

DDO 126	# of holes	% of global on average per hole type	% of global in total per hole type
Type 1 Hα	3	0.113	0.339
Type 2 Hα	0	0.00	0.00
Type 3 Hα	1	0.732	0.732
All Holes Hα	4		1.07
Type 1 HI	3	2.14	6.42
Type 2 HI	0	0.00	0.00
Type 3 HI	1	0.263	0.263
All Holes HI	4		6.68

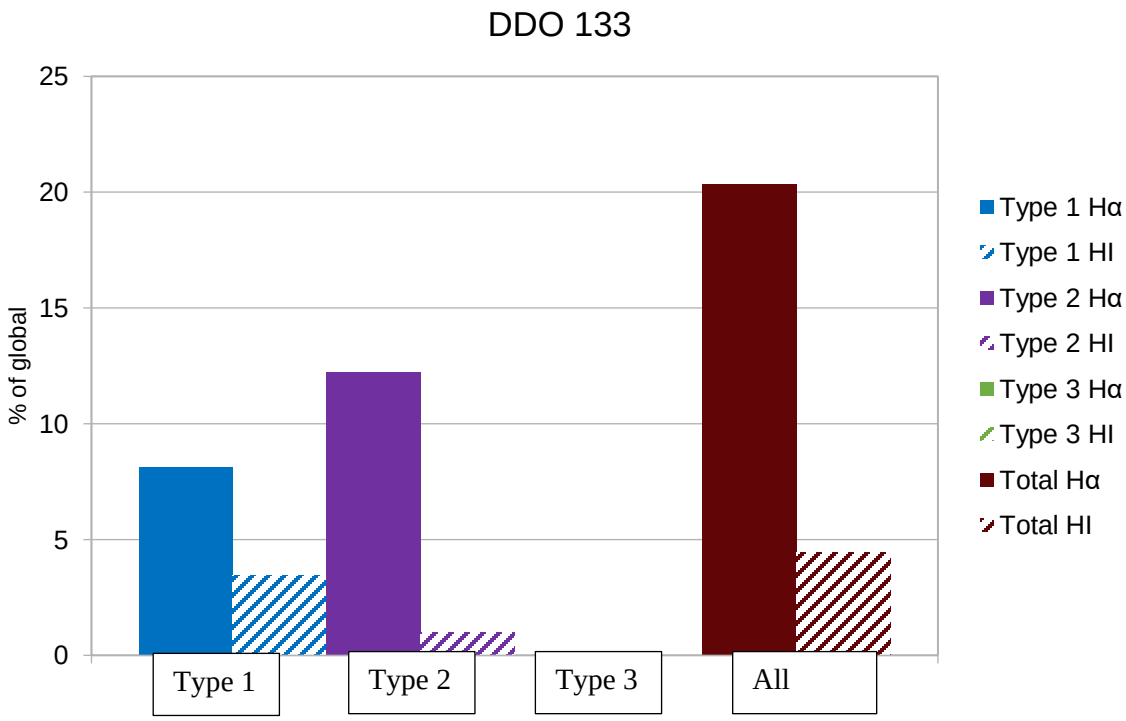

Figure 18: DDO 133 global percentage of Ha (solid) and HI (striped) contained in the rings.

Table 12: DDO 133 ring characteristics.

DDO 133	# of holes	% of global on average per hole type	% of global in total per hole type
Type 1 Hα	4	2.03	8.13
Type 2 Hα	1	12.2	12.2
Type 3 Hα	…	…	…
All Holes Hα	5		20.3
Type 1 HI	4	0.865	3.46
Type 2 HI	1	0.979	0.979
Type 3 HI	…	…	...
All Holes HI	5		4.44

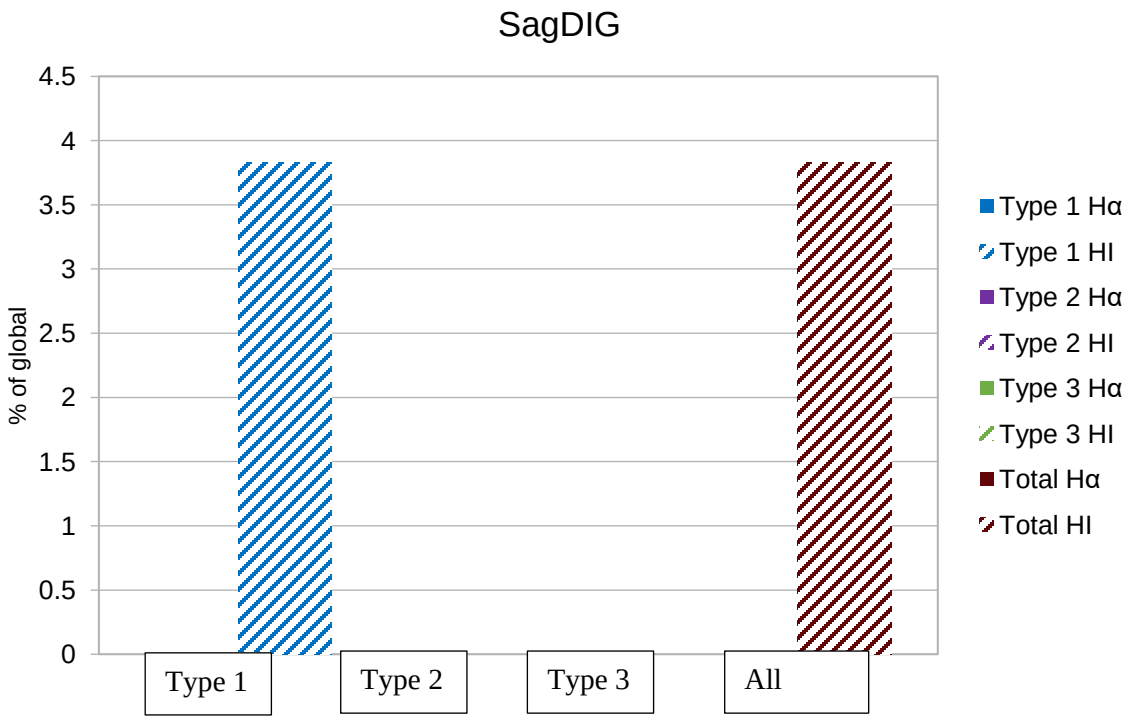

Figure 19: SagDIG global percentage of Ha (solid) and HI (striped) contained in the rings.

Table 13: SagDIG ring characteristics.

SagDIG	# of holes	% of global on average per hole type	% of global in total per hole type
Type 1 Hα	1	0.00	0.00
Type 2 Hα	…	…	…
Type 3 Hα	…	…	…
All Holes Hα	1		0.00
Type 1 HI	1	3.83	3.83
Type 2 HI	…	…	…
Type 3 HI	…	…	…
All Holes HI	1		3.83

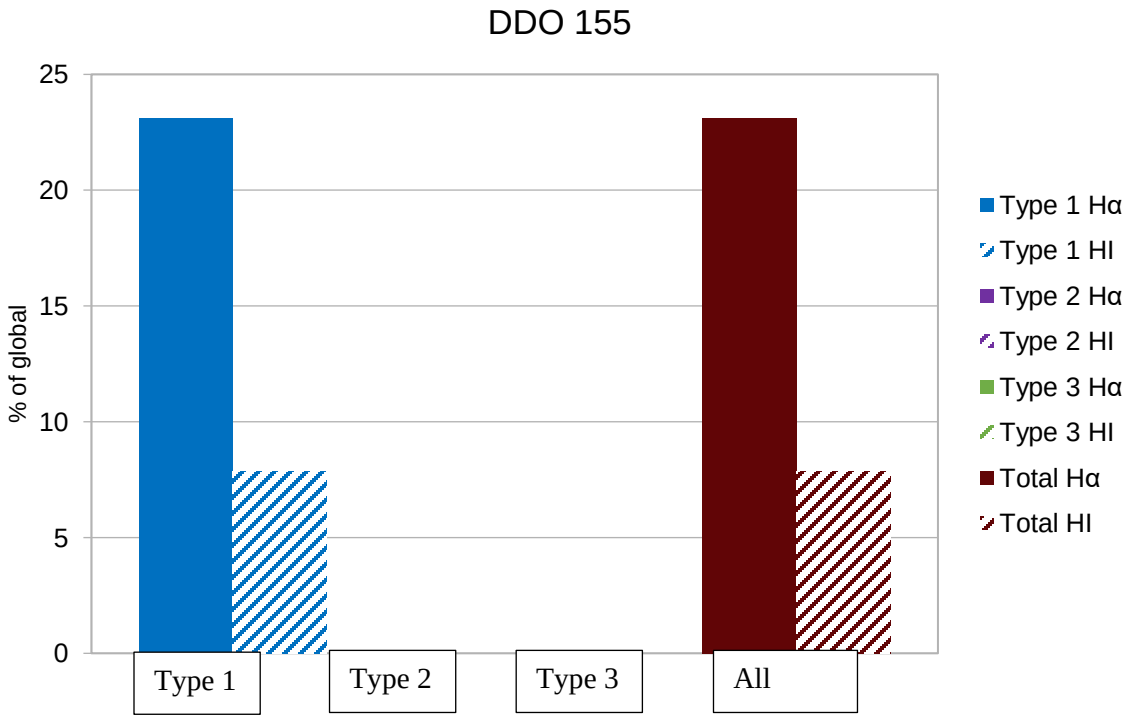

Figure 20: DDO 155 global percentage of Ha (solid) and HI (striped) contained in the rings.

Table 14: DDO 155 ring characteristics.

DDO 155	# of holes	% of global on average per hole type	% of global in total per hole type
Type 1 Hα	3	7.70	23.1
Type 2 Hα	…	…	…
Type 3 Hα	…	…	…
All Holes Hα	3		23.1
Type 1 HI	3	2.59	7.85
Type 2 HI	…	…	…
Type 3 HI	…	…	…
All Holes HI	3		7.85

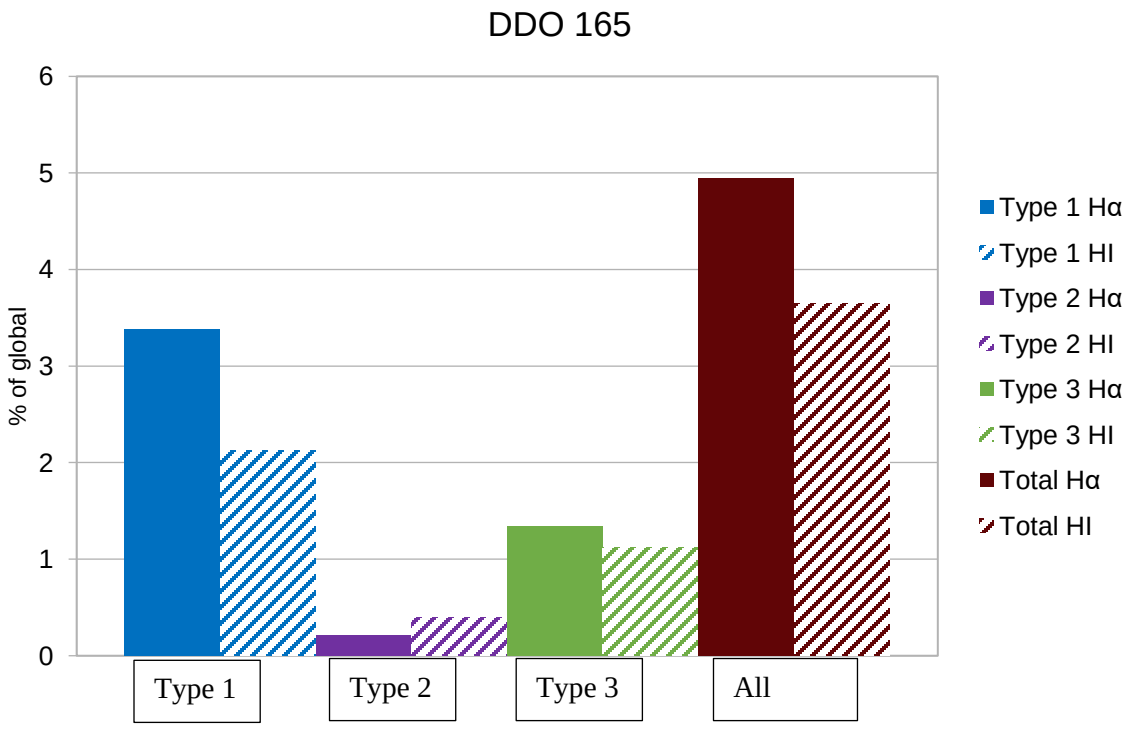

Figure 21: DDO 165 global percentage of Ha (solid) and HI (striped) contained in the rings.

Table 15: DDO 165 ring characteristics.

DDO 165	# of holes	% of global on average per hole type	% of global in total per hole type
Type 1 Hα	1	3.38	3.38
Type 2 Hα	1	0.219	0.219
Type 3 Hα	1	1.35	1.35
All Holes Hα	3		4.95
Type 1 HI	1	2.13	2.13
Type 2 HI	1	0.399	0.399
Type 3 HI	1	1.12	1.12
All Holes HI	3		3.65

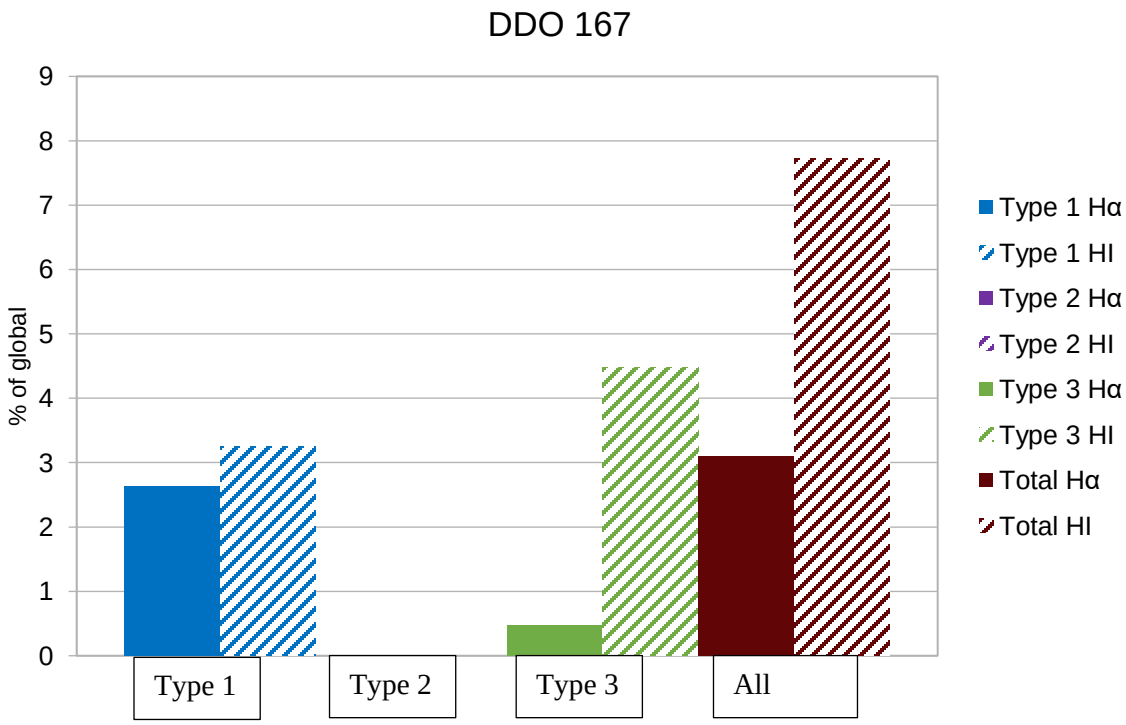

Figure 22: DDO 167 global percentage of Ha (solid) and HI (striped) contained in the rings.

Table 16: DDO 167 ring characteristics.

DDO 167	# of holes	% of global on average per hole type	% of global in total per hole type
Type 1 Hα	2	1.36	2.72
Type 2 Hα	…	…	…
Type 3 Hα	1	0.497	0.497
All Holes Hα	3		3.22
Type 1 HI	2	1.48	3.25
Type 2 HI	…	…	…
Type 3 HI	1	4.47	4.47
All Holes HI	3		7.72

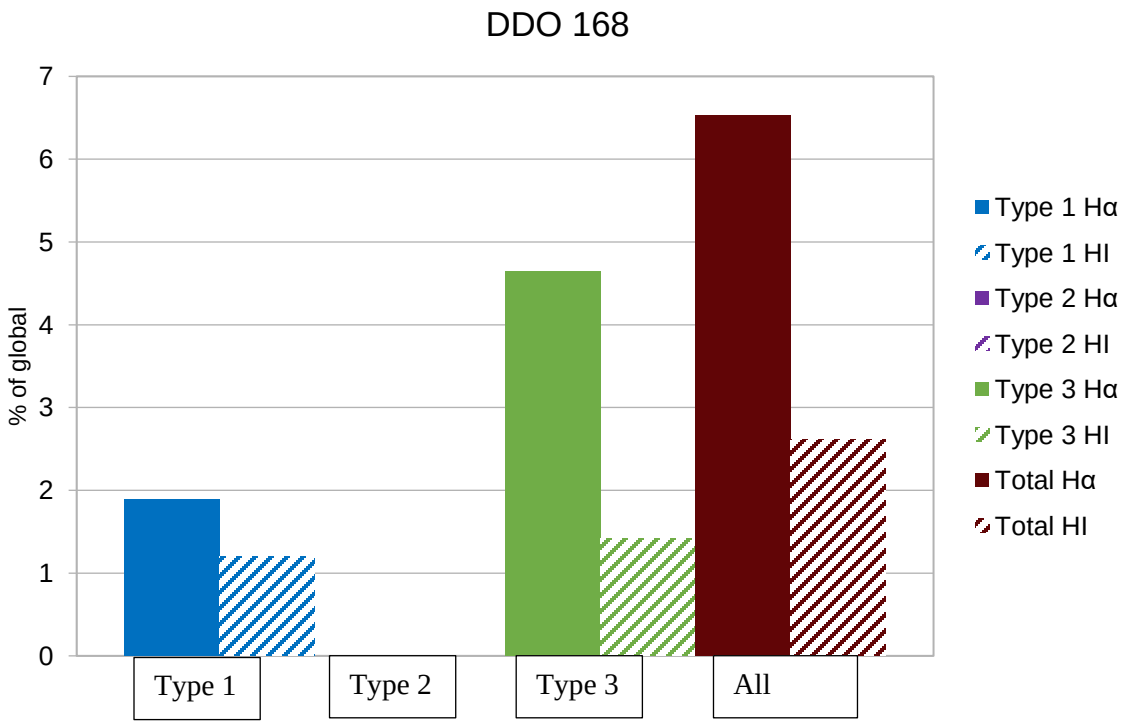

Figure 23: DDO 168 global percentage of Ha (solid) and HI (striped) contained in the rings.

Table 17: DDO 168 ring characteristics.

DDO 168	# of holes	% of global on average per hole type	% of global in total per hole type
Type 1 Hα	1	1.89	1.89
Type 2 Hα	…	…	…
Type 3 Hα	1	4.64	4.64
All Holes Hα	2		6.53
Type 1 HI	1	1.20	1.20
Type 2 HI	…	…	…
Type 3 HI	1	1.42	1.42
All Holes HI	2		2.62

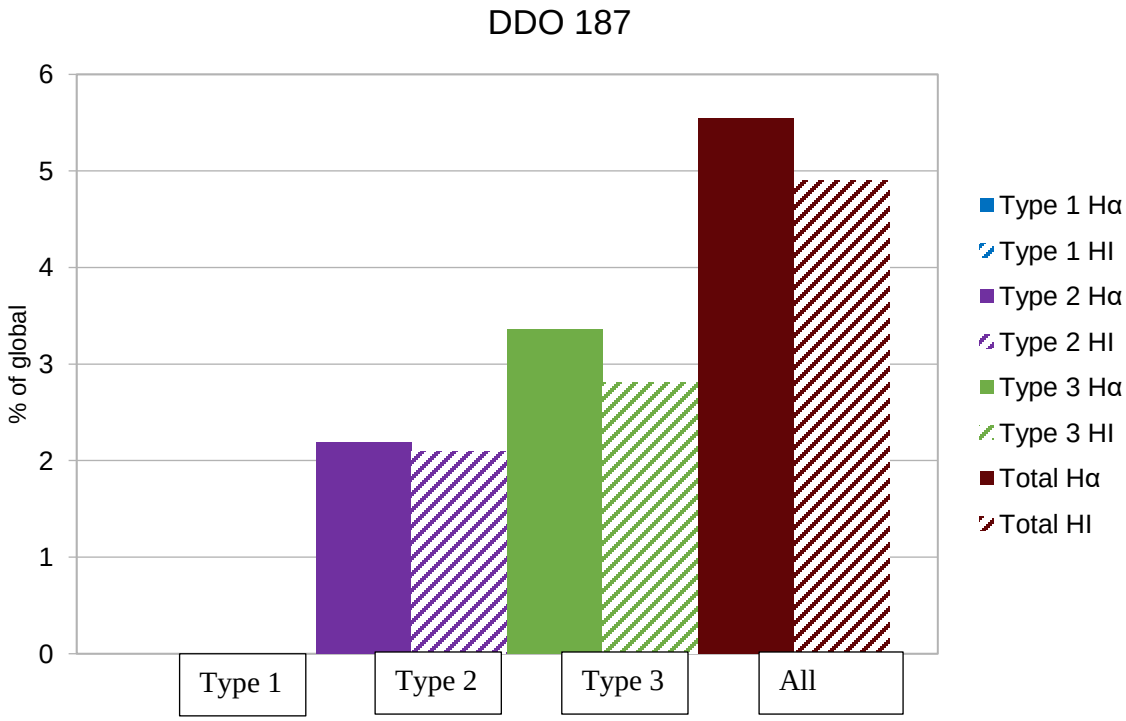

Figure 24: DDO 187 global percentage of Ha (solid) and HI (striped) contained in the rings.

Table 18: DDO 187 ring characteristics.

DDO 187	# of holes	% of global on average per hole type	% of global in total per hole type
Type 1 Hα	…	…	…
Type 2 Hα	1	2.19	2.19
Type 3 Hα	2	1.68	3.36
All Holes Hα	3		5.55
Type 1 HI	…	…	…
Type 2 HI	1	2.09	2.09
Type 3 HI	2	1.35	2.81
All Holes HI	3		4.44

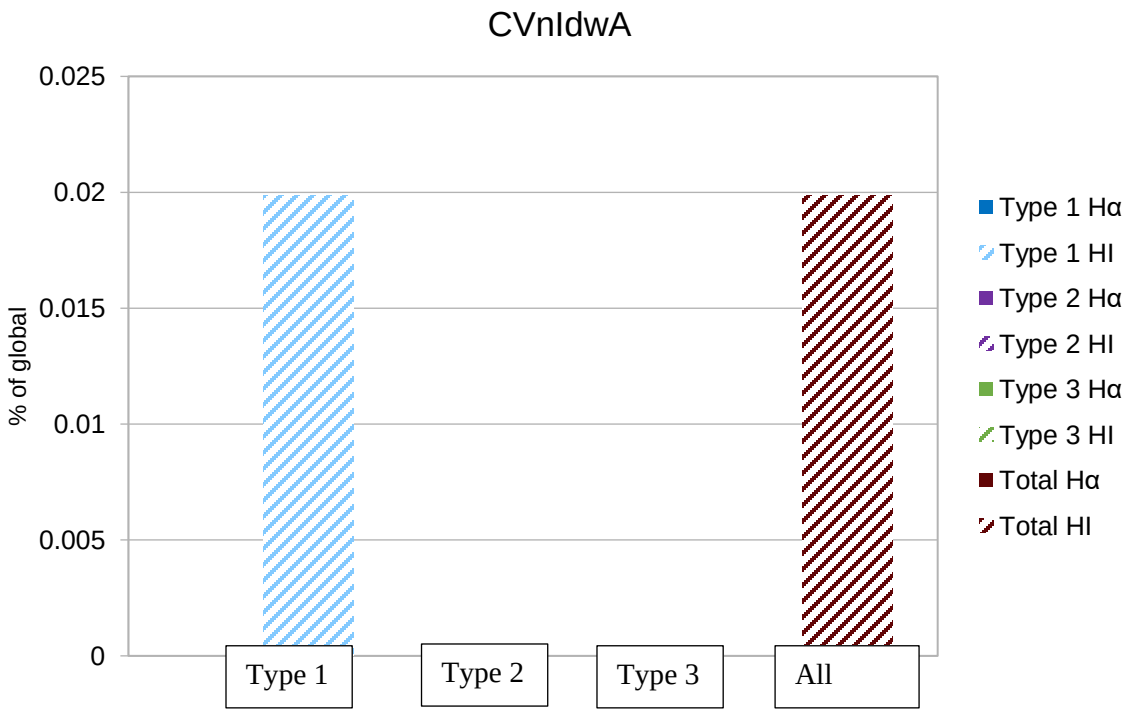

Figure 25: CVnIdwA global percentage of Ha (solid) and HI (striped) contained in the rings.

Table 19: CVnIdwA ring characteristics.

CVnIdwA	# of holes	% of global on average per hole type	% of global in total per hole type
Type 1 Hα	1	0.00	0.00
Type 2 Hα	…	…	…
Type 3 Hα	…	…	…
All Holes Hα	1		0.00
Type 1 HI	1	0.0199	0.0199
Type 2 HI	…	…	…
Type 3 HI	…	…	…
All Holes HI	1		0.0199

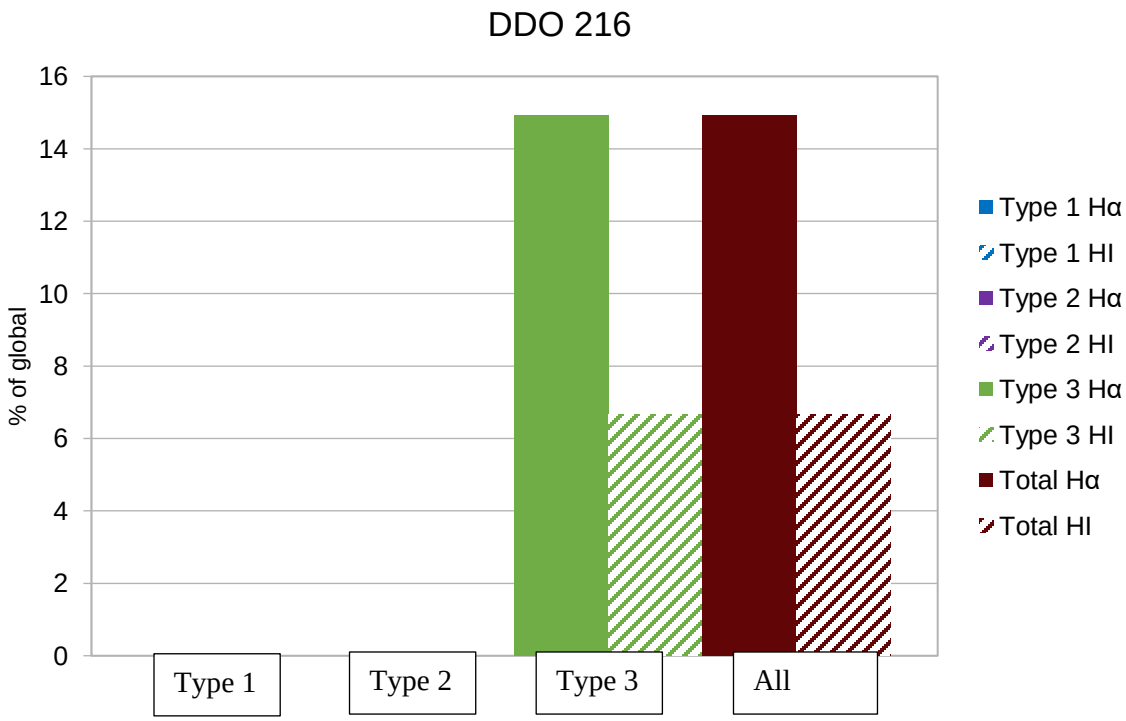

Figure 26: DDO 216 global percentage of Ha (solid) and HI (striped) contained in the rings.

Table 20: DDO 216 ring characteristics.

DDO 216	# of holes	% of global on average per hole type	% of global in total per hole type
Type 1 Hα	…	…	…
Type 2 Hα	…	…	…
Type 3 Hα	3	4.97	14.9
All Holes Hα	3	N/A	14.9
Type 1 HI	…	…	…
Type 2 HI	…	…	…
Type 3 HI	3	2.26	6.66
All Holes HI	3	N/A	6.66

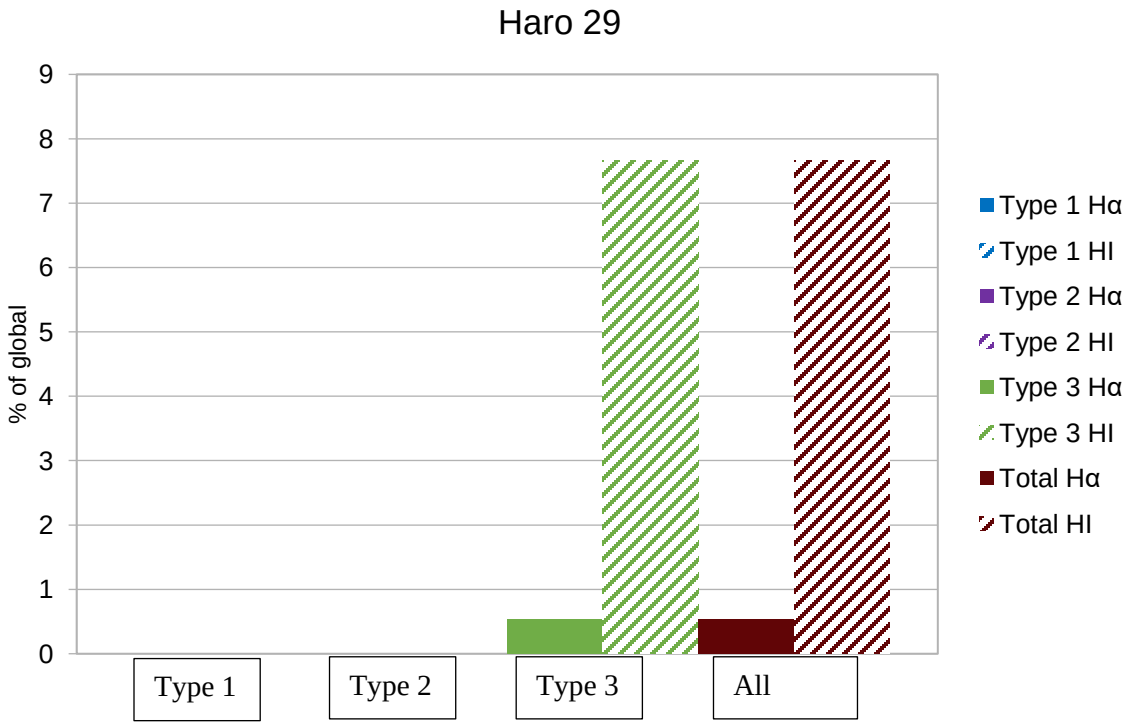

Figure 27: Haro 29 global percentage of Ha (solid) and HI (striped) contained in the rings.

Table 21: Haro 29 ring characteristics.

Haro 29	# of holes	% of global on average per hole type	% of global in total per hole type
Type 1 Hα	…	…	…
Type 2 Hα	…	…	…
Type 3 Hα	2	0.0994	0.199
All Holes Hα	2	N/A	0.199
Type 1 HI	…	…	…
Type 2 HI	…	…	…
Type 3 HI	2	3.03	7.66
All Holes HI	2	N/A	7.66

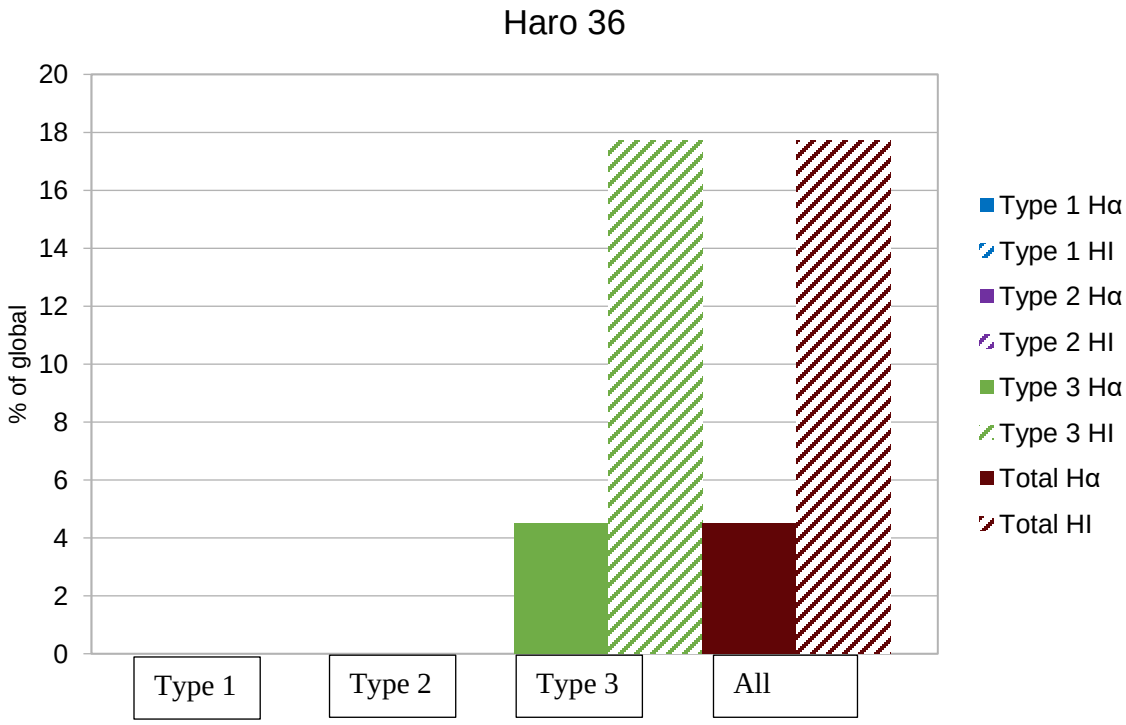

Figure 28: Haro 36 global percentage of Ha (solid) and HI (striped) contained in the rings.

Table 22: Haro 36 ring characteristics.

Haro 36	# of holes	% of global on average per hole type	% of global in total per hole type
Type 1 Hα	…	…	…
Type 2 Hα	…	…	…
Type 3 Hα	1	4.51	4.51
All Holes Hα	1	N/A	4.51
Type 1 HI	…	…	…
Type 2 HI	…	…	…
Type 3 HI	1	17.7	17.7
All Holes HI	1	N/A	17.7

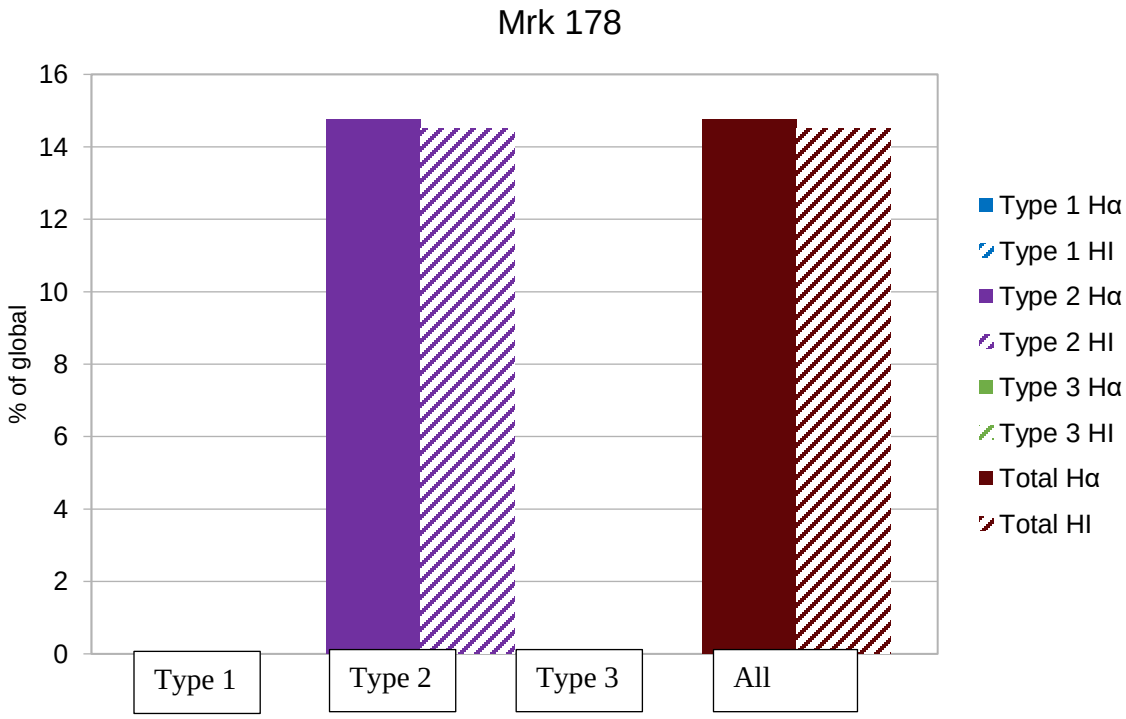

Figure 29: Mrk 178 global percentage of Ha (solid) and HI (striped) contained in the rings.

Table 23: Mrk 178 ring characteristics.

Mrk 178	# of holes	% of global on average per hole type	% of global in total per hole type
Type 1 Hα	…	…	…
Type 2 Hα	1	14.8	14.8
Type 3 Hα	…	…	…
All Holes Hα	1	N/A	14.8
Type 1 HI	…	…	…
Type 2 HI	1	14.5	14.5
Type 3 HI	…	…	…
All Holes HI	1	N/A	14.5

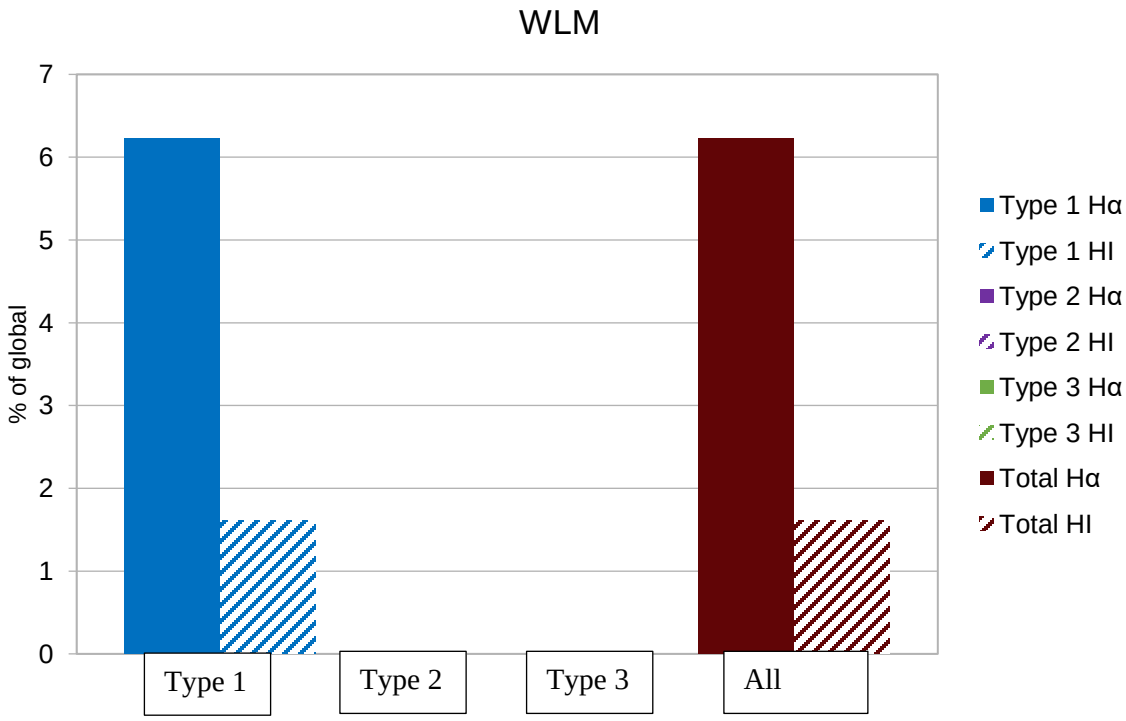

Figure 30: WLM global percentage of Ha (solid) and HI (striped) contained in the rings.

Table 24: WLM ring characteristics.

WLM	# of holes	% of global on average per hole type	% of global in total per hole type
Type 1 Hα	4	1.56	6.24
Type 2 Hα	…	…	…
Type 3 Hα	…	…	…
All Holes Hα	4	N/A	6.24
Type 1 HI	4	0.403	1.61
Type 2 HI	…	…	…
Type 3 HI	…	…	…
All Holes HI	4	N/A	1.61

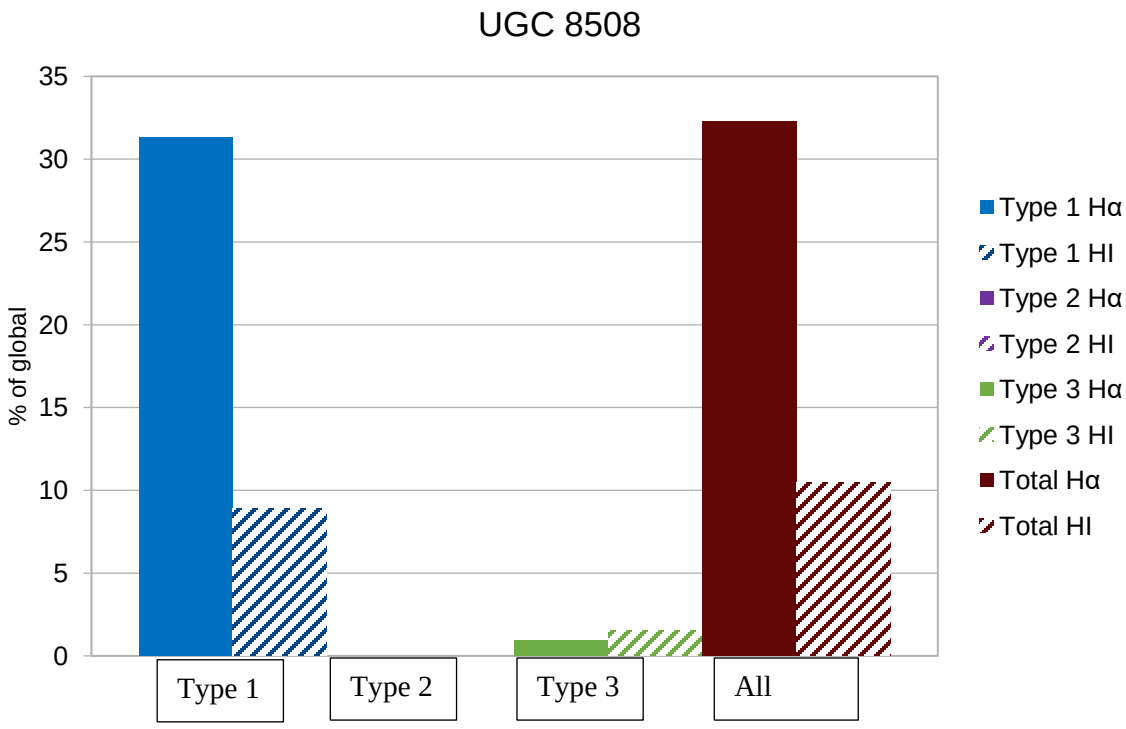

Figure 31: UGC 8508 global percentage of Ha (solid) and HI (striped) contained in the rings.

Table 25: UGC 8508 ring characteristics.

UGC 8508	# of holes	% of global on average per hole type	% of global in total per hole type
Type 1 Hα	1	31.3	31.3
Type 2 Hα	…	…	…
Type 3 Hα	2	0.480	0.960
All Holes Hα	3	N/A	32.3
Type 1 HI	1	8.90	8.90
Type 2 HI	…	…	…
Type 3 HI	2	0.869	1.55
All Holes HI	3	N/A	10.5

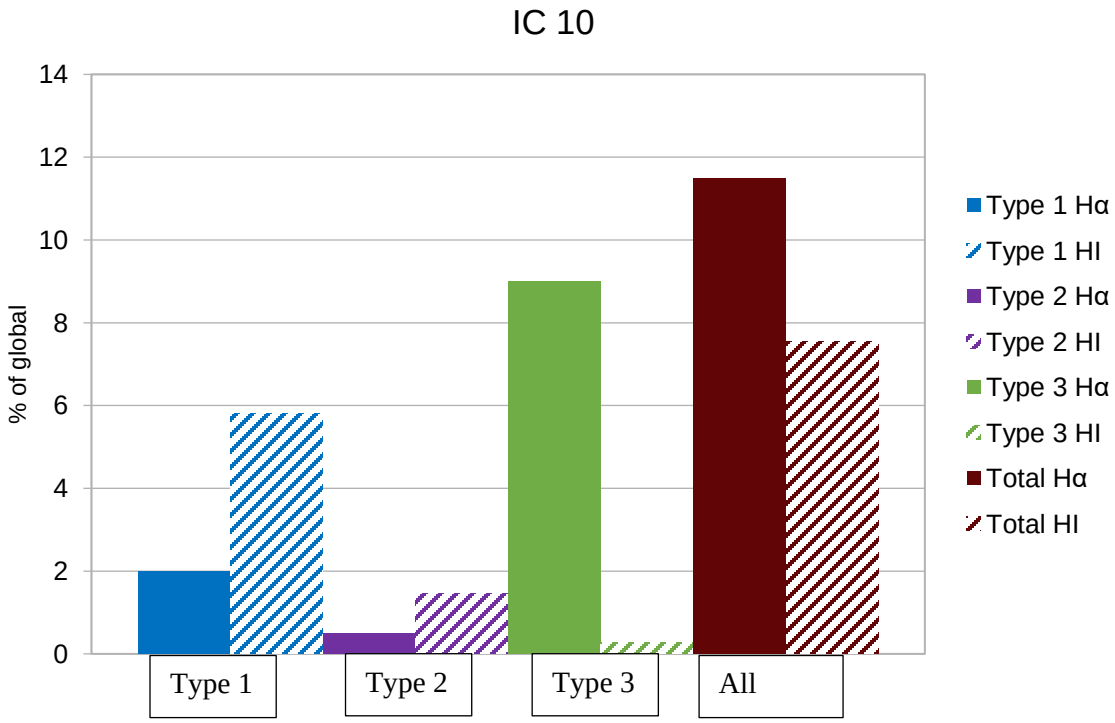

Figure 32: NGC 3738 global percentage of Ha (solid) and HI (striped) contained in the rings.

Table 26: IC 10 ring characteristics.

IC 10	# of holes	% of global on average per hole type	% of global in total per hole type
Type 1 Hα	14	0.882	2.07
Type 2 Hα	5	0.00847	0.512
Type 3 Hα	1	.913	9.13
All Holes Hα	20	N/A	11.7
Type 1 HI	14	0.426	5.82
Type 2 HI	5	0.292	1.46
Type 3 HI	1	0.281	0.281
All Holes HI	20	N/A	7.56

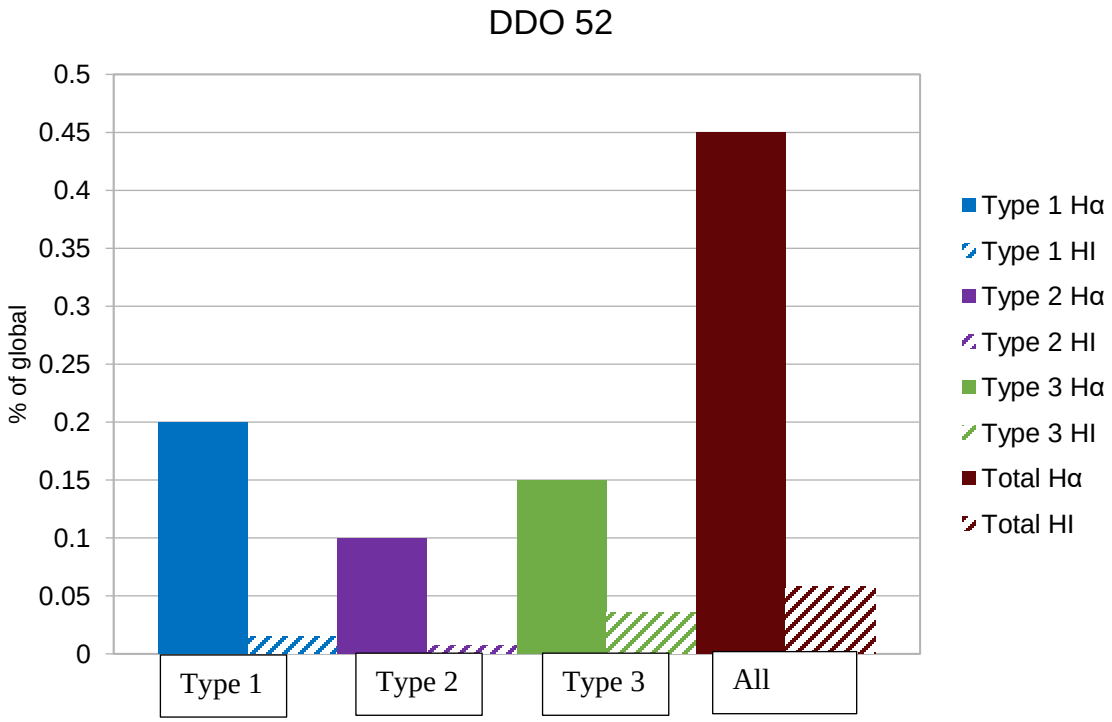

Figure 33: DDO 52 global percentage of Ha (solid) and HI (striped) contained in the rings.

Table 27: DDO 52 ring characteristics.

DDO 52	# of holes	% of global on average per hole type	% of global in total per hole type
Type 1 Hα	5	0.0431	0.200
Type 2 Hα	6	0.0168	0.101
Type 3 Hα	6	0.0255	0.151
All Holes Hα	17	N/A	.452
Type 1 HI	5	0.0829	0.414
Type 2 HI	6	0.00126	0.00755
Type 3 HI	6	0.00588	0.0353
All Holes HI	17	N/A	0.0580

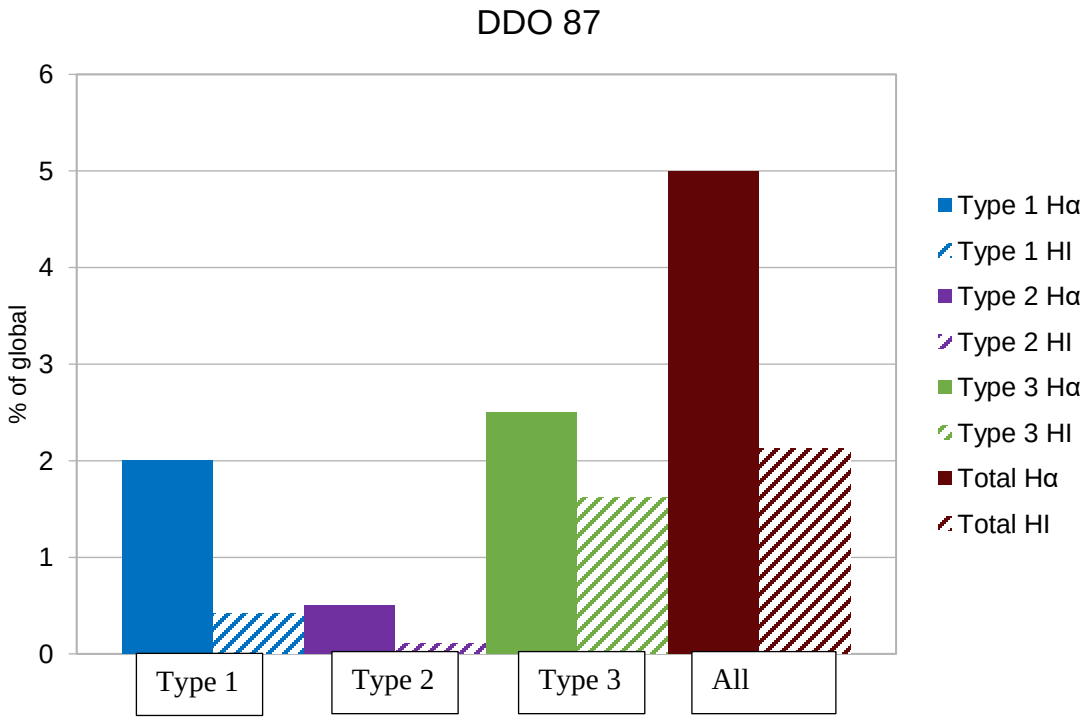

Figure 34: DDO 87 global percentage of Ha (solid) and HI (striped) contained in the rings.

Table 28: DDO 87 ring characteristics.

DDO 87	# of holes	% of global on average per hole type	% of global in total per hole type
Type 1 Hα	5	.444	2.22
Type 2 Hα	7	0.00721	0.505
Type 3 Hα	6	.393	2.36
All Holes Hα	18	N/A	5.09
Type 1 HI	5	0.0829	0.414
Type 2 HI	7	0.00147	0.103
Type 3 HI	6	0.268	1.61
All Holes HI	18	N/A	2.13

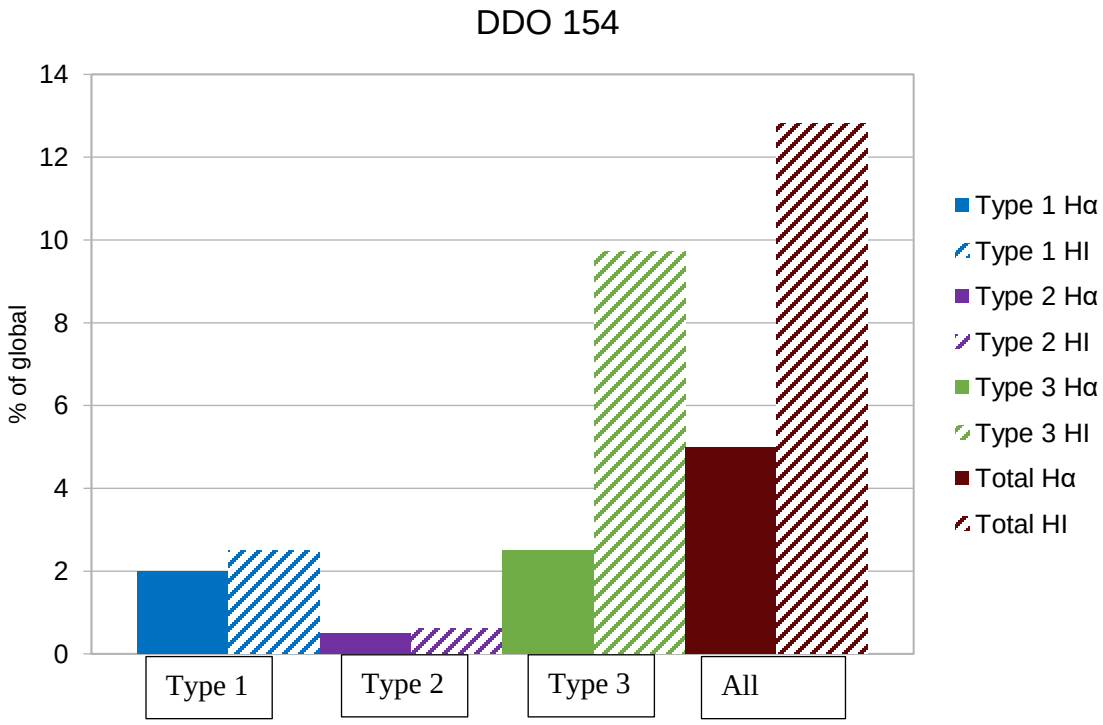

Figure 35: DDO 154 global percentage of Ha (solid) and HI (striped) contained in the rings.

Table 29: DDO 154 ring characteristics.

DDO 154	# of holes	% of global on average per hole type	% of global in total per hole type
Type 1 Hα	5	0.0424	2.12
Type 2 Hα	2	0.269	0.534
Type 3 Hα	2	1.26	2.51
All Holes Hα	9	N/A	5.16
Type 1 HI	5	0.499	2.49
Type 2 HI	2	0.312	0.623
Type 3 HI	2	4.86	9.71
All Holes HI	9	N/A	12.8

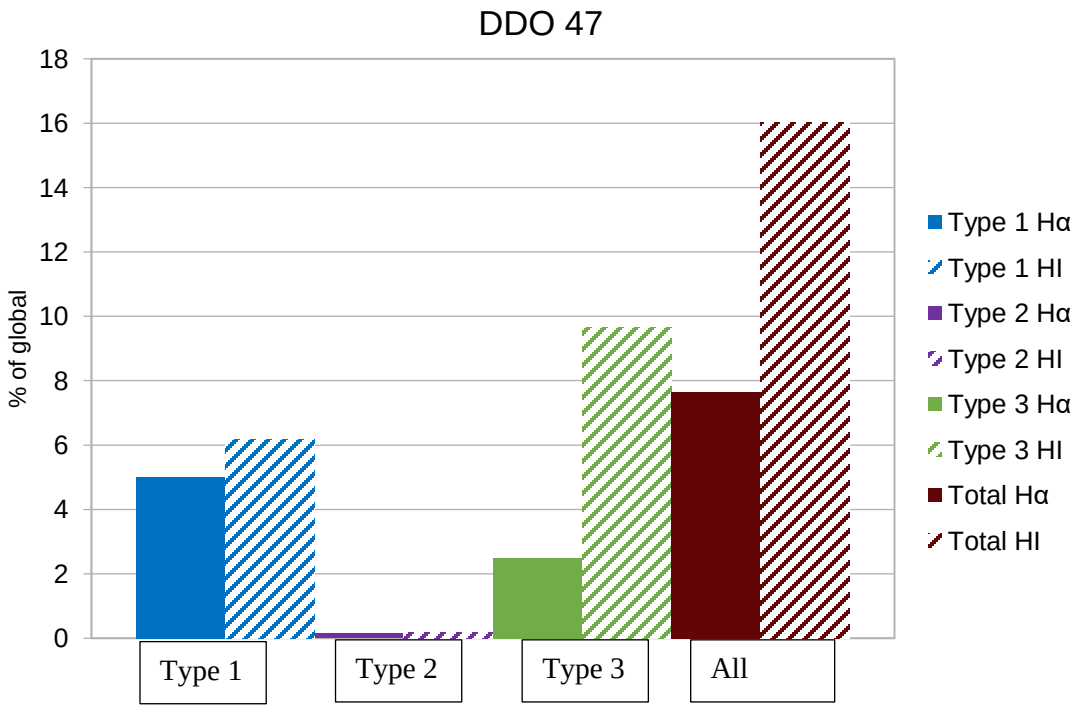

Figure 36: DDO 47 global percentage of Ha (solid) and HI (striped) contained in the rings.

Table 30: DDO 47 ring characteristics.

DDO 47	# of holes	% of global on average per hole type	% of global in total per hole type
Type 1 Hα	10	0.555	5.55
Type 2 Hα	5	0.031	0.151
Type 3 Hα	4	.643	2.57
All Holes Hα	19	N/A	6.97
Type 1 HI	10	0.620	6.19
Type 2 HI	5	0.0372	0.186
Type 3 HI	4	2.43	9.65
All Holes HI	19	N/A	16.0

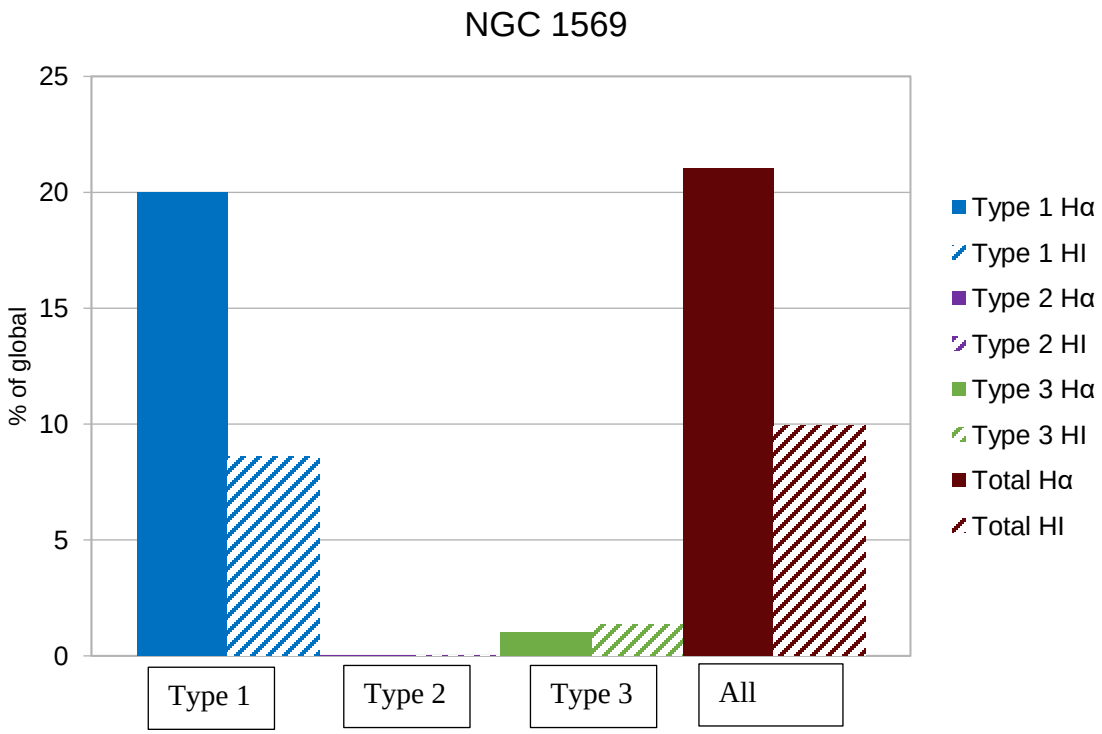

Figure 37: NGC 1569 global percentage of Ha (solid) and HI (striped) contained in the rings.

Table 31: NGC 1569 ring characteristics.

NGC 1569	# of holes	% of global on average per hole type	% of global in total per hole type
Type 1 Hα	3	6.90	20.7
Type 2 Hα	1	0.022	0.022
Type 3 Hα	1	1.01	1.01
All Holes Hα	5	N/A	21.7
Type 1 HI	3	2.87	8.61
Type 2 HI	1	0.00861	0.00861
Type 3 HI	1	1.34	1.34
All Holes HI	5	N/A	9.96

2. DISCUSSION

As seen in Part III, section 1, there are histograms comparing the global galactic star formation rates to the star formation in the rings by hole type and also summed together. While looking at each of the galaxies individually we do not see any noticeable correlation between the hole type and the amount of star formation occurring in the rings, but this could be more carefully studied in a future project.

When we take each of the galaxies and compare their ring compositions (Figure 38) we can see that majority of the galaxies have relatively low amounts of HI and star formation rate (SFR) (Case 4) in the rings compared to their global amounts (roughly < 10%). As a reminder, we have defined four cases: Case 1 where both the HI and SFR ring fractions are high (High-High), Case 2: High HI, Low SFR (High-Low), Case 3: Low HI, High SFR (Low-High); and Case 4: Low HI, Low SFR (Low-Low).

Two galaxies, UGC 8508 and Mrk 178 fall into Case 1 relative to the rest of the sample, and so are candidates for having star-induced star formation be an important mechanism for star formation in these galaxies. It is also worth noting that NGC 1569 lies on the cusp of Case 1 and Case 2. This is consistent with its classification as a post starburst galaxy with expanding shells [2, 6] it is a candidate for star-induced star formation in the recent past.

Case 2 (High-Low) and Case 3 (Low-High) both contain five and four galaxies each, respectively. Without knowing the age of each hole, it is hard to infer where along the stage of star development the rings are. These galaxies

could potentially be towards the beginning stages of star formation (Case 2, High-Low) and final stages of star formation (Case 3, Low-High). Although for Case 2 with lower levels of star formation, star-induced star formation is not an important star formation mechanism in these galaxies now, if the holes are shown to be relatively young, then it is possible that there has not yet been time for star formation to have been initiated in the HI shells around the holes. For Case 3, with relatively high amounts of the global star formation occurring in the rings, it would seem that the presence or creation of the holes is an important mechanism for star formation in these galaxies, although the lack of HI needs further examination. For example, if the holes are shown to be relatively old, this would suggest that the HI in the rings has been used up for star formation leading us to believe that star-induced star formation.

Case 4 (Low-Low) seems to be where majority of the galaxies in this study tend to fall. All except two galaxies (CVnIdwA and SagDIG) in this case do have some HI and star formation in the rings, but below 10% of the galactic star formation is in the rings in these galaxies. Because of this it is difficult to say whether or not star-induced star formation occurred in these galaxies but it is not a major mechanism right now. This indicates that other mechanisms such as turbulence in the ISM are causing most of the star formation in the majority of our sample of dwarf galaxies.

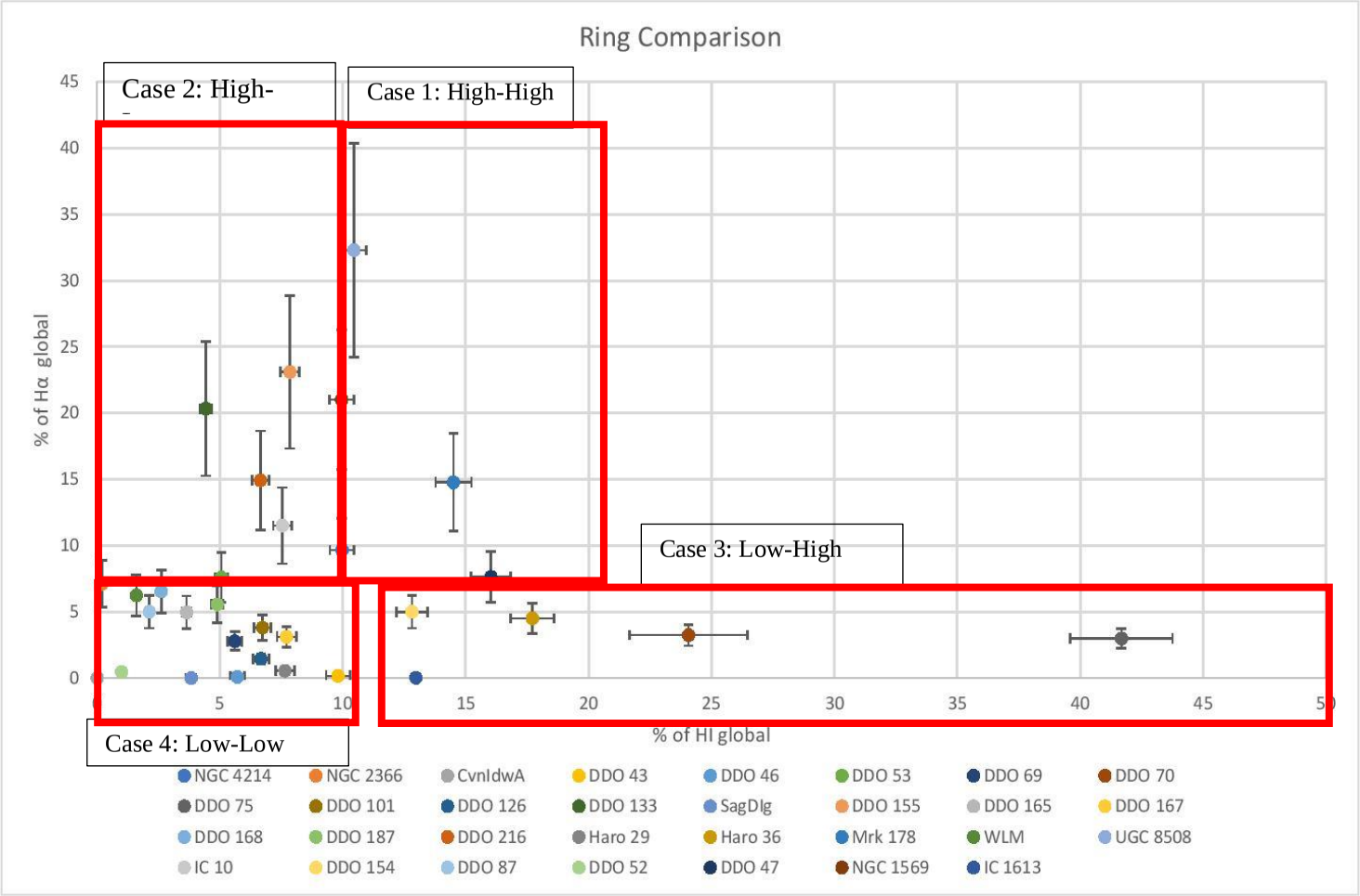

Figure 38: A scatterplot showing the global comparison of each galaxies Hα (y-axis) vs HI (x-axis).

IV. CONCLUSION AND FUTURE WORK

1. CONCLUSION

This research is the continuation of the LITTLE THINGS project's goal of understanding dwarf galaxies and star formation. The purpose of this thesis is to study the importance of triggered star formation in the simple systems of dwarf galaxies. In specific, we looked at the contents of the rings possibly formed from prior star formation events such as supernovae of OB associations in dwarf galaxies to determine the importance of star-induced star formation. Our results show that star-induced star formation is likely an important factor in a few of our dwarf galaxies where the rings contained a relatively high amount of the global star formation in the galaxies. For the majority of the sample, it does not appear to be an important mechanism operating at this time. This indicates that other processes, such as turbulence, are currently a larger factor in the star formation we see in dwarf galaxies today.

2. FUTURE WORK

Based on the results that were obtained in this study, further research could indicate whether or not star-induced star formation may have occurred or might occur in our dwarf galaxy sample. Examining the ages of holes would allow for us to see if those galaxies HI-rich rings but little/no star formation have young holes and so might not yet have time to induce star formation in the rings. If the holes are old, then that would indicate that no star formation has been induced at any time and so that mechanism is not occurring. For galaxies with

active star formation now but HI-poor rings, if they are old, this would be consistent with induced star formation that has had time to consume, ionize, or blow out the HI from the rings. If the holes are young, it is puzzling how star formation could be occurring with little raw material and this would require closer examination on a hole-by-hole basis. There may be localized regions of HI enhancement which are supporting the existing star formation. For Case 4 galaxies, with low levels of HI and star formation, if the holes are young then star-induced star formation is not an important operating process in these galaxies and other processes are dominant. If the holes are old, there is no way to tell whether star-induced star formation has ever occurred, however.

This research could be done initially using the kinetic ages of the holes determined by Pokhrel [2]. For some galaxies, even more in-depth studies using optical data could help to determine the age of the stellar populations inside the holes that presumably helped created them (similar to the work done by Zhang et al. [7]).

Further studies of DDO 50, a well-studied dwarf galaxy, could also prove fruitful as there are several studies addressing the formation of the HI holes and shells, and star formation regions, in this galaxy. Pokhrel [2] has found 41 HI holes, not all of which have been examined in these previous works.

References

[1] Hunter, D.A & Elmegreen B.G., Star Formation Properties of a Large Sample of Irregular Galaxies, The Astronomical Journal 128 (2004), no. 5, 2170–2205.

[2] Pokhrel, N. (2016). HI Structure and Kinematics of the Interstellar Medium in LITTLE THINGS Galaxies, PhD. Diss, Florida International University.

[3] Prialnik, D. (2000). An Introduction to the Theory of Stellar Structure and Evolution. Cambridge University Press. 195–212. ISBN 0-521-65065-8.

[4] Mo, H., Van den Bosch, F. & White, S. (2010). Galaxy Formation and Evolution. Cambridge University Press.

[5] Castor, J., McCray, R. & Weaver, R., Interstellar Bubbles. The Astrophysical Journal, Letters, 200: L107–L110, September 1975.

[6] Walter, F.; Brinks, E. Holes and Shells in the Interstellar Medium of the Nearby Dwarf Galaxy IC 2574. Astron. J. 1999, 118, 273–301.

[7] Zhang, H.; Hunter D.A.; Elmegreen B.G., Gao, Y. & Schruba, A., Outside-In Shrinking of the Star-Forming Disk of Dwarf Irregular Galaxies, The Astronomical Journal 143 (2012), no. 2, 47.

[8] Vorobyov E.I. & Basu. S., Numerical Simulations of Expanding Supershells in Dwarf Irregular Galaxies. II. Formation of Giant HI Rings. Astronomy & Astrophysics, 431:451–464, February 2005.

[9] Federrath C., The Turbulent Formation of Stars, Physics Today 71 (2018), no. 6, 38–42.

[10] Martin C.D., Fanson, J.; Schiminovich, D.; Morrissey, P.; Friedman, P.G., et al., The Galaxy Evolution Explorer: A Space Ultraviolet Survey Mission, The Astrophysical Journal 619 (2005), no. 1, L1–L6.

[11] Bagetakos, I., Brinks, E., Walter, F., de Blok, W. J. G., Usero, A., Leroy, A.K., Rich, J.W., & Kennicutt Jr., R. C., The Fine-Scale Structure of the Neutral

[12] Sparke, L. S.; Gallagher III, J. S. (2000). Galaxies in the Universe: An Introduction. Cambridge University Press. ISBN 978-0-521-59740-1.

[13] Palma, C., “The Process of Star Formation.” The Process of Star Formation | Astronomy 801: Planets, Stars, Galaxies, and the Universe, www.e-education.psu.edu/astro801/content/l5_p3.html.

[14] Williams, J. P.; Blitz, L.; McKee, C. F. (2000). "The Structure and Evolution of Molecular Clouds: from Clumps to Cores to the IMF". Protostars and Planets IV. p. 97.

[15] Shaver, P. A., McGee, R. X., Newton, L.M., Danks, A.C., Pottasch, S.R., The galactic abundance gradient, Monthly Notices of the Royal Astronomical Society, Volume 204, Issue 1, September 1983, Pages 53–112.

[16] Interstellar Medium in Nearby Galaxies. The Astronomical Journal, 141:23, January 2011.

[17] Chandrasekhar, S. (1958) [1939]. An Introduction to the Study of Stellar Structure. New York: Dover. ISBN 978-0-486-60413-8.

[18] Hunter, D.A. & Elmegreen B.G., Broadband Imaging of a Large Sample of Irregular Galaxies. The Astrophysical Journal, Supplement, 162:49–79, January 2006.

[19] Elmegreen, D.M. (1998). Galaxies and Galactic Structure. Prentice Hall. ISBN 978-0-137-79232-0

[20] Massari, D., Breddels, M.A., Helmi, A. *et al.* Three-Dimensional Motions in the Sculptor Dwarf Galaxy as a Glimpse of a New Era. *Nat Astron* **2,** 156–161 (2018).

[21] Cox, N., editor (2000). Allen's Astrophysical Quantities. New York: Springer-Verlag. ISBN 0-387-98746-0.

[22] Stahler, S. W. & Palla, F. (2004). The Formation of Stars. Weinheim: Wiley-VCH. ISBN 3-527-40559-3.

[23] Webb, J. R. (2016). Extragalactic Astrophysics. Morgan & Claypool Publishers. ISBN 978-1-681-74410-0